
UNIVERSITY OF
BIRMINGHAM

# ASSESSMENT OF THE TOXICITY OF LIPID NANOCAPSULES AND POLYMER NANOPARTICLES ON A NEURONAL CELL MODEL AS A FIRST STEP TOWARDS THEIR DEVELOPMENT FOR NOSE-TO-BRAIN DRUG DELIVERY

by

**RIFKA NURUL UTAMI**

**A thesis submitted to the University of Birmingham for the degree of**

**MASTER OF SCIENCE**

**SCHOOL OF PHARMACY**

**INSTITUTE OF CLINICAL SCIENCES**

**COLLEGE OF MEDICAL AND DENTAL SCIENCES**

**UNIVERSITY OF BIRMINGHAM**

**October 2018**

## ABSTRACT

Nose-to-brain delivery is a promising alternative to deliver therapeutics to the central nervous system, due to the possibility to bypass the blood-brain barrier. Because of their versatility, nanoparticulate delivery systems may offer several advantages for this route. This study investigates the correlation between physicochemical characteristics of two different types of nanomaterials, namely lipid nanocapsules (LNCs) and PLGA nanoparticles (PLGA-NPs), and their behaviour towards SH-SY5Y cells as the neuronal cell model. Physicochemical characterisation and stability studies showed that all the formulations exhibited excellent properties and stability under storage (4 $^{o}$C) and physiological conditions. Surface hydrophobicity was also assessed wherein PLGA-NPs were found to be generally more hydrophobic compared to LNCs. Cytotoxicity assays towards SH-SY5Y cells suggested that surfactant-related toxicity is more likely to occur in LNCs compared to PLGA-NPs. Cellular uptake was also analysed using flow cytometry and fluorescence microscopy. The results from this study can be used as consideration in developing nanoparticulate delivery system for nose-to-brain delivery.

## ACKNOWLEDGMENT

I would like to take this opportunity to express my biggest gratitude to Indonesian Endowment Fund for Education (LPDP RI) for the financial sponsorship to carry out this project here in the University of Birmingham.

I would also like to convey my gratefulness to my supervisors, Dr. Marie-Christine Jones and Dr. Hanene Ali-Boucetta for the outstanding guidance and assistance. All the things that I have learned from them I perceive as very valuable treasure for my future career development.

My thanks and appreciations also go to all my colleagues in Pharmacy Research Laboratory for the generous support and companionship throughout the project.

At last but not the least, I am most indebted to my parents, my two sisters, and my greatest friend, Aat Prayogo Muhtar, for the unconditional love and support that help me through completing this programme.

# List of Abbreviations

| | |
|---|---|
| **AFM** | *Atomic force microscopy* |
| **AUC** | *Area under curve* |
| **BBB** | *Blood-brain barrier* |
| **CMC** | *Critical micelle concentration* |
| **CNS** | *Central nervous system* |
| **DLS** | *Dynamic light scattering* |
| **DMSO** | *Dimethyl sulfoxide* |
| **DPBS** | *Dulbecco's phosphate buffered saline* |
| **FBS** | *Foetal bovine serum* |
| **GA** | *Glycolic acid* |
| **HI** | *Heat inactivated* |
| **HIC** | *Hydrophobic interaction chromatography* |
| **HS** | *Hydroxystearate* |
| **IN** | *Intranasal* |
| **IV** | *Intravenous* |
| **LA** | *Lactic acid* |
| **LDE** | *Laser Doppler electrophoresis* |
| **LNC** | *Lipid nanocapsule* |
| **MCC** | *Mucociliary clearance* |
| **MCT** | *Medium chain triglyceride* |
| **MWCO** | *Molecular weight cut-off* |
| **NP** | *Nanoparticle* |

| | |
|---|---|
| **OEC** | *Olfactory ensheathing channel* |
| **PBS** | *Phosphate buffered saline* |
| **PCL** | *Poly-ε-caprolactone* |
| **PCS** | *Photon correlation spectroscopy* |
| **PdI** | *Polydispersity index* |
| **PEG** | *Polyethylene glycol* |
| **PEO** | *Polyethylene oxide* |
| **PLA** | *Poly lactic acid* |
| **PLGA** | *Poly-lactic-co-glycolide* |
| **PPO** | *Polypropylene oxide* |
| **PS** | *Polystyrene* |
| **PVA** | *Polyvinyl alcohol* |
| **PVAc** | *Polyvinyl acetate* |
| **RI** | *Refractive index* |
| **SAT** | *Salt aggregation test* |
| **SEM** | *Scanning electron microscopy* |
| **SPC** | *Soy phosphatidylcholine* |
| **TEM** | *Transmission electron microscopy* |
| **TJ** | *Tight junction* |

# Table of Contents

# List of Figures

# List of Tables

# 1. Introduction

## 1.1 Nose-to-brain delivery

The treatment of diseases of the central nervous system (CNS) remains a great challenge for scientists worldwide. The terms "CNS disease" includes a variety of conditions such as Alzheimer's Disease, Parkinson's Disease, headache disorders, strokes, multiple sclerosis, infections, and cancer. Two of the aforementioned conditions, Alzheimer's disease and strokes, are amongst leading causes of mortality and morbidity worldwide (1, 2) and are likely to continue to represent a public health concern due to a rapidly aging population. The treatments available are often only partially effective, mainly due to issues in achieving therapeutic concentrations at the site of action within the brain, rather than a simple lack of suitable active pharmaceutical ingredients (1-4).

As the main organ of the human CNS, the brain has its whole anatomy protected by a sophisticated system, to maintain its integrity and function. This protective role is fulfilled, at least partly, by a structure called the blood-brain-barrier (BBB). The BBB is a selectively permeable membrane that prevents exogenous substances, such as drug molecules, from entering the brain, while facilitating the passage of important nutrients (5). The BBB consists of a complex system of endothelial cells, astrocytes, pericytes, and basal lamina (Figure 1) (6). In contrast to endothelial cells in other parts of the body, brain endothelia have a specific arrangement in which the cells strongly adhere to each other, forming tight junctions (TJs). The presence of TJs makes it nearly impossible for exogenous hydrophilic substances to enter the brain tissue by concentration-dependent diffusion through paracellular transport. Such molecules will be prevented from accumulating in the brain, unless they can bind to transporter proteins meant to facilitate the entry of nutrients, such as glucose and peptides (5-7).

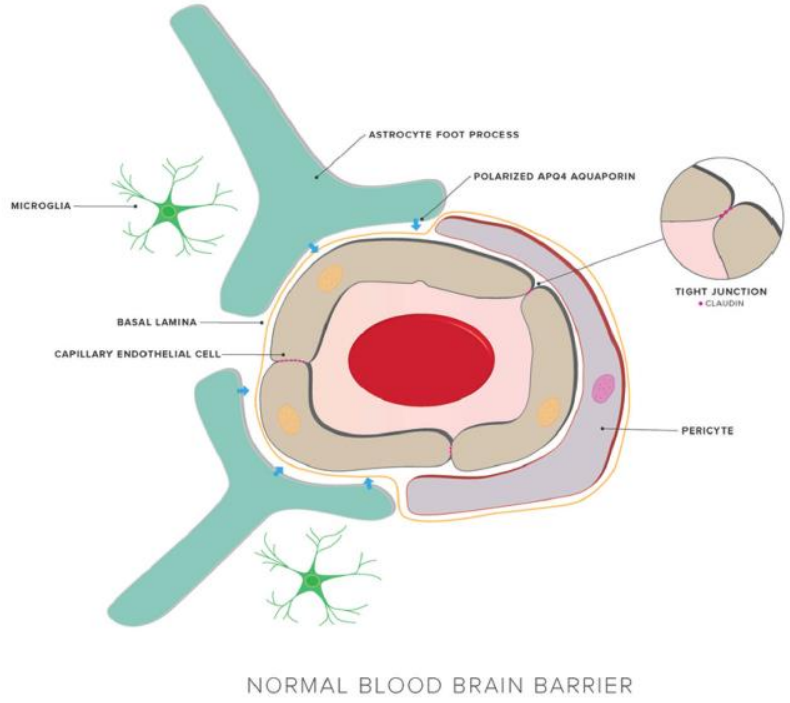


**Figure 1.** Structure of BBB in human; used with permission from Journal of Neurosurgery Publishing Group (6)

Generally, drug molecules need to be lipophilic and less than 500 Da in size in order to pass through the BBB. Therefore, it follows that none of the larger drug molecules can penetrate the BBB, especially biologicals. Surprisingly, ca. 98% of hydrophobic, low-molecular-weight drugs (≤500 Da) still face problem achieving therapeutic concentrations in the brain, despite having suitable physico-chemical properties. This is mainly due to the presence of efflux transporters along the BBB, including the P-glycoprotein, which pump drugs out of cells (5), but also to metabolism by enzymes, such as flavin-dependent oxygenases, monoamine oxidases, reductases, hydrolases, etc (8-10). For that reason, several methods, either invasive or non-invasive, have been tested to increase the amount of drug reaching the brain. Invasive methods mostly involve temporary disruption of BBB integrity, for example osmotic- and ultrasound-based method (11, 12). However, these methods possess great risks as they may also

permit the entry of other hazardous, infectious or toxic materials (13). Thus, non-invasive methods are still preferred.

More recently, alternatives routes of administration have been explored to gain entry to the brain, with the nose-to-brain delivery route being particularly promising (14). Nose-to-brain delivery relies on administration of the formulation to the olfactory region and, to a lesser extent, the trigeminal nerve as both regions are exposed to the external environment and connects to the CNS directly. This provides the possibility to bypass the BBB and consequently enhance the amount of drug reaching the brain tissues. The euphoric effect after nasal administration of cocaine is the long-known proof of this direct pathway from nasal cavity to the brain. Chow *et al.* (15) conducted a study in rats to compare cocaine concentration in different regions in the brain compared to the blood plasma after intranasal (IN) and intravenous (IV) administration. They have shown that after 1-minute, the olfactory-bulb-to-plasma cocaine ratio following IN administration was three times the IV ratio. Westin *et al.* (16) also found that 0-5 minutes post-administration of morphine in rats, the brain hemisphere/plasma area under curve (AUC) ratio was significantly higher when administered IN rather than IV. Also, a recent study using mice as animal model by Hada *et al*. (17) demonstrated a higher brain level of imatinib, a tyrosine kinase inhibitor used as an anticancer agent, following IN administration compared to IV injection.

A small number of human studies have also been carried out in recent years, although it is more difficult to establish a correlation between nasal administration and brain accumulation in humans due to ethical issues. Instead, studies rely on observing behavioural changes in the volunteers after IN administration or by sampling the cerebrospinal fluid as a proxy for the brain (18). Numerous studies assessing the efficacy of intranasally administrated oxytocin, a neuropeptide, had been carried out this past decade through observation of behavioural changes

post-treatment in human volunteers (19, 20). In another study, Born *et al.* (21) demonstrated that IN administration of neuropeptides (melanocortin(4-10), insulin, and vasopressin) produced high peptide concentrations in the cerebrospinal fluid but not in the plasma level, indicating a direct transport to the CNS.

At the moment, there is a lack of consensus among scientists about whether nose-to-brain delivery occurs through a single mechanism or combination of the pathways (Figure 2) (14, 22). Out of all possibilities, it is believed that two pathways play a major role in nose-to-brain delivery: 1) the olfactory and 2) the trigeminal nerve pathways. The olfactory nerve endings are located in the olfactory region of the nose and terminate in the corresponding region in the temporal lobe of the brain. This olfactory region can be found in the upper part of the nasal cavity, just beneath the cribriform plate (Figure 3). Although it is known that the olfactory region in humans is less developed than in some animals (e.g. rodents), the outer layer of the region possesses microvilli which increase the surface area available for drug absorption (9). Meanwhile, trigeminal nerves are located in both the respiratory and olfactory regions, connecting the nasal cavity to the brain stem (22).

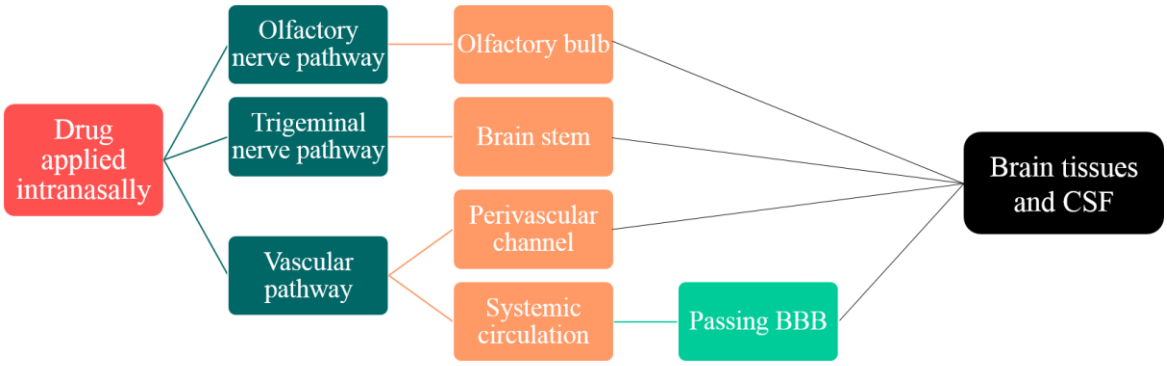


**Figure 2.** Possible routes for a drug to be transported to the brain following IN administration (22)

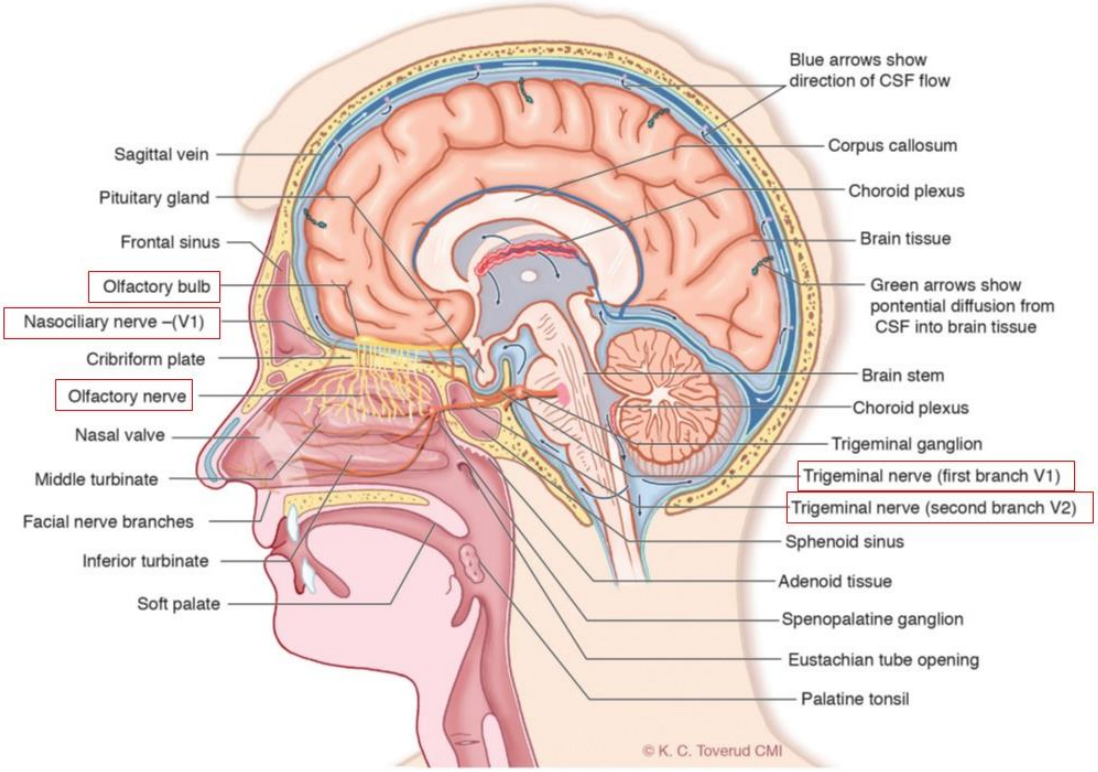


**Figure 3**. Lateral section of the human nose and brain showing key anatomical structures involved in nose-to-brain delivery, used with permission from Future Science and K. C. Toverud CMI (13)

At first glance, one might assume that nose-to-brain delivery occurs solely through inter-axonal transport. However, this cannot explain the 'rapid and direct' transport of drug molecules, since inter-axonal transport is a slow process that may take hours and days to be completed (13). Another possibility is for the drug to be transported to the lamina propria, located beneath the mucosal layers, either paracellularly or transcellularly (14). Inside the lamina propria, drug molecules can be delivered to the brain through various mechanisms, including the rapid transport through the channel formed by olfactory ensheathing cells (OECs). Overall, the exact mechanism of transport and subsequent distribution in the brain is difficult to predict. Yet, it is clear that nose-to-brain delivery provides an opportunity to deliver drugs to different regions of the brain, allowing for the possibility of targeted delivery for localised diseases such as Parkinson's Disease or brain tumours (22).

## 1.2 Nanoparticles for nose-to-brain delivery

Advancement in science and technology has allowed nanotechnology to become an emerging field in many aspects. Research into biomedical nanomaterials (1-1000 nm) has grown significantly over the past decades and these materials continue to attract interest due to their versatility. The main advantage of the small size of nanoparticles is the ability to enhance cellular uptake (23), slow down clearance (24) and protect the molecules from degradation (25), thus increasing the amount of drug reaching the target organ or tissue.

Depending on the raw materials used, nanomaterials can be categorised as organic and inorganic nanoparticles; organic nanomaterials can be manufactured out of lipids, proteins or polymers, while gold and silver are commonly used in the synthesis of inorganic nanomaterials. Because of the nature of the ingredients used in their preparation, organic nanomaterials are generally considered to be less toxic compared to its inorganic counterpart (26).

In the context of nose-to-brain administration, nanoparticulate delivery systems can offer numerous advantages. For example, encapsulation could increase the residence time in the nasal cavity and enhance the amount of drug reaching the CNS (10, 27). However, one needs to ensure that the formulation is administered to the right location in the nasal cavity, in order to minimise the systemic absorption of the nanoformulations (13). Indeed, nanoparticles have been used to increase IN drug transport and while this could ultimately improve brain accumulation, this will only happen if the nanoparticles are able to cross the BBB. If targeted delivery to the brain is the end goal, it might be necessary to tailor the properties of the nanoparticles to favour one mode of transport over the other so that the drug accumulates in the desired region of the brain, depending on the condition being treated (10). Nevertheless, numerous studies had been carried out providing the evidence of nanoparticle efficacy for nose to brain delivery in the recent years. For instance, Sekerdag *et al*. (28) had demonstrated the

efficacy of lipid-PEG-PLGA nanoparticles to treat glioblastoma following intranasal administration in rats. El-Zaafarany *et al*. (29), also observed an improved brain targeting capacity, this time using oxcarbazepine loaded in lipidic emulsomes, a nanocarrier with a lipid core shielded with phospholipids. Despite evidence of efficacy, questions remain at the end about whether a particular type of nanoparticles or the drug alone would be transported to the brain following IN administration. If this is the case, toxicity assessment of the nanoparticle should be taken as a first step to ensure the biocompatibility of the formulation (30). Hence, a toxicological evaluation of two types of nanomaterials, namely lipid nanocapsules (LNCs) and poly(lactic-co-glycolid acid) (PLGA) particles was undertaken in this project as a first step towards their optimisation for nose-to-brain drug delivery.

## 1.3 Lipid nanocapsules (LNCs)

Lipid-based nanomaterials are some of the most extensively studied nanomaterials because of their biocompatibility and versatility. Liposomes remain the best examples of clinically-effective lipid-based nanomaterials and there are now several drug formulations on the market (31). Liposomes' efficacy as drug carriers is attributed to their ability to enhance membrane penetration because of the characteristic of phospholipids as the main ingredient that mimics the cellular membrane (32). Also, the amphiphilic nature of phospholipids allows liposomes to be able to entrap both water-soluble and oil-soluble drugs, albeit to different extents (33). However, liposomes possess some drawbacks, such as the need for organic solvents during production and potential issues with stability and complement activation (34).

Recently, another lipid-based system has been promoted for drug delivery. Lipid nanocapsules (LNCs), developed by Heurtault *et al*. (patent no.US2009/0238865A1), are composed mainly of medium-chain triglycerides as the oily core and a mixture of a surfactant

and phospholipids as the shell; together, these ingredients form a semi-rigid structure (Figure 4) that is a hybrid between liposomes and polymeric nanoparticles (35). Another interesting characteristic of LNCs is the possibility to control the obtained size by varying the composition, although proportions need to be kept within a specific range, to ensure that true LNCs are obtained. The range of concentrations for each ingredient was found to be 10 – 40% for the hydrophilic surfactant, 10 – 25% for the oil (triglyceride), and 35 – 80 % for the external aqueous phase. Outside this range, no clear (nano)structure will be formed (36-38). It is important to note that increasing the surfactant and oil concentration will lead to smaller and larger LNCs.

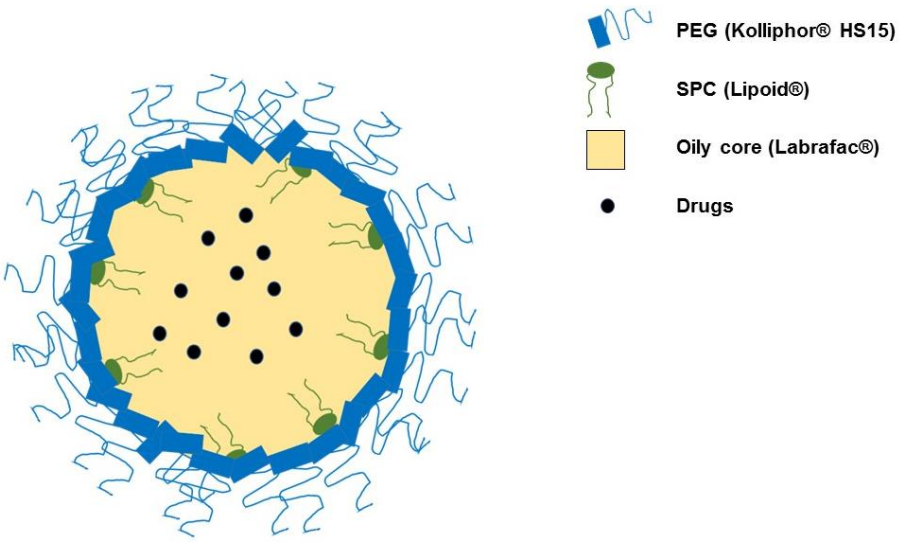


**Figure 4**. Schematic representation of the structure of lipid nanocapsule; adapted with modification from Huynh, *et al.* (35)

Kolliphor® HS15, PEG-based surfactant functionalised with hydroxystearate chain (Figure 5) is most commonly used in the manufacture of LNCs. The presence of this high-density PEG on nanocapsule surface is beneficial for both colloidal and storage stability (36). The PEG coating can also help to mask nanoparticles from phagocytic cells (39), leading to prolonged circulation times (40, 41). However, toxicity issues may arise because of high

surfactant concentrations. Indeed, the amphiphilic nature of the surfactant can allow it to interact with the cellular membrane, causing membrane disruption (42, 43). Thus, purification is an important step for LNC production.

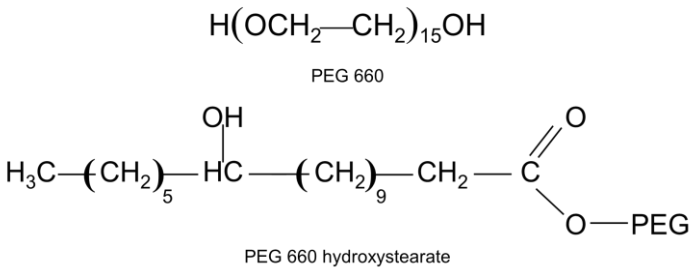


**Figure 5**. Chemical structure of Kolliphor® HS15 consisting of PEG 660 and PEG 660-HS (41)

So far, LNCs have mostly been studied on cancer models, either *in vitro* or using animal studies (35). The findings confirmed the efficacy and beneficial aspects of LNCs used as nanoparticulate delivery systems. Here, LNCs were selected as a potential nose-to-brain delivery system because of their promising characteristics, including excellent stability and versatility.

## 1.4 PLGA nanoparticles (PLGA-NPs)

While LNCs are a relatively recent example, biodegradable polymeric nanoparticles have been studied for drug delivery for a number of years. In theory, these nanoparticles offer great promise due to their lack of toxicity. Most commonly, biodegradable nanomaterials are obtained from polymers such as poly-ɒ,ɬ-lactide-co-glycolide (PLGA), poly-lactic acid (PLA), and poly-ε-caprolactone (PCL) (44) with PLGA often being the most preferred (45). There are different types of PLGA polymers, based on the ratio of lactide and glycolide which later governs the distinct characteristics of each type, such as crystallinity and hydrophobicity. For

instance, PLGA with a higher glycolide content is more amorphous, while a higher lactide content makes PLGA more crystalline, more hydrophobic and more slowly degraded (46).

PLGA-NPs can be prepared by several methods: 1) nanoprecipitation, 2) emulsion/solvent evaporation, 3) interfacial deposition, and 3) emulsification-diffusion. Generally, all these methods involve mixing the organic phase containing the polymer into an aqueous phase in the presence of a stabiliser. Out of the methods listed above, nanoprecipitation is the most commonly used to prepare PLGA nanoparticles. Nanoprecipitation involves dissolving the polymer in a water-miscible organic solvent (e.g. methanol, acetone) which is then added dropwise into the aqueous phase. Nanoparticles are formed when the organic solvent is left to evaporate under constant stirring (46-48).

Most formulations use poly(vinyl alcohol) as the stabiliser. Here, triblock copolymers consisting of PPO (polypropylene oxide) and PEO (polyethylene oxide) chains (Figure 6), have been selected to prepare stable, stealth, PEGylated particles (49-51). Additionally, one type of poloxamer, namely poloxamer 188, has demonstrated the ability to transiently increase the permeability of the mucosal layer (52). This can be favourable for the development of intranasal delivery system for brain targeting. Because of their compatibility, PLGA-NPs can be proposed as another potential nanoparticulate system for nose-to-brain delivery. Besides, the distinct characteristics between PLGA-NPs and LNCs can provide additional information on the impact of composition on the effect of nanoparticles *in vitro*, or specifically in this study, their effect towards neuronal cell model.

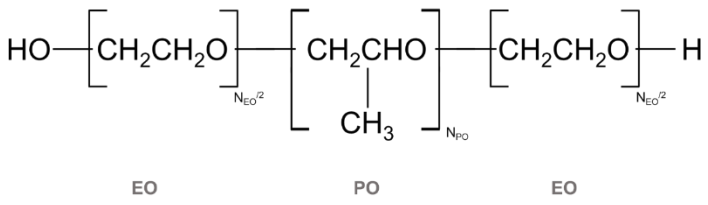


***Figure 6.*** *Chemical structure of poloxamer composed of PPO and PEO block* (53)

## 1.5 Aims and objectives

From several possible administration routes for brain delivery, the nose-to-brain route is considered the most promising. The olfactory region in the nasal cavity is known as the only portion exposed to external environment that connects to the CNS. This offers the possibility to bypass the BBB and consequently enhance the amount of drug reaching the brain tissue (9). This study was designed as the first step for finding the most suitable nanocarrier system for nose-to-brain delivery. Two types of nanocarriers, LNCs and PLGA-NPs are going to be assessed for their characteristics and interaction with neuronal cells. The results obtained will be analysed to find out if there is any correlation between the characteristics of the nanoparticles (size and surface chemistry) and their effect *in vitro*. This study has been designed to test the following research hypotheses:

1. There is a size-dependence in the interaction between nanoparticles and cells including cytotoxicity and uptake, where smaller nanoparticles are expected to have greater effect in both cases.
2. There is a correlation between nanoparticle surface hydrophobicity and both stability of the colloidal systems and the cellular uptake of the nanomaterials.

**Objectives:**

1. Manufacture of LNCs and PLGA-NPs and their characterisation by dynamic light scattering (size; surface hydrophobicity through salting-out method), electrophoretic mobility (zeta potential), and hydrophobic interaction chromatography (surface hydrophobicity.
2. Cytotoxicity assessment of the manufactured nanoparticles towards SH-SY5Y cells using MTT assay.
3. Analysis of nanoparticle cellular uptake using fluorescent LNCs and PLGA-NPs using flow cytometry and fluorescence microscopy.

# 2. Nanoparticle manufacturing and characterisation

## 2.1 Introduction

Nanoparticle characterisation represents an important step following their manufacture. Generally, methods are used to assess the particles' physicochemical properties, including, but not limited to, particle size, surface properties and morphology. These properties dictate, not only the behaviour of the nanoparticles in a pharmaceutical formulation, but also their efficacy and potential toxicity as drug delivery system (54, 55). The effect of size on the fate of nanoparticles has been demonstrated by various researchers. Most of the findings suggest that smaller sizes increase the cellular uptake of nanoparticles (56, 57) but may also increase their cytotoxicity (58, 59). Additionally, particle size also has an impact on triggering the immune response. In this case, larger particles are more likely to be recognised by the phagocytic cells and to induce an inflammatory reaction (60, 61). For that reason, during the development of nanoparticles as drug carriers, it is important for researchers to find the right particle size to achieve optimal efficacy and minimum toxicity.

Particle size measurements can be carried out using different analytical approaches, such as dynamic light scattering (DLS) or microscopy, namely transmission electron microscopy (TEM), scanning electron microscopy (SEM), and atomic force microscopy (AFM) (54). DLS remains the most common technique used and has the advantages of being fast and to allow the measurement to be performed in solution. DLS is based on the detection of fluctuations in the scattering of light by colloidal particles subjected to Brownian motion. This signal can then be correlated to the hydrodynamic diameter of the particles. In addition to information of size, DLS also provides data on size distribution, in the form of the polydispersity index (PdI), to assess the uniformity of the particle population (62), with the caveat that only spherical particles can be analysed. Microscopic methods can be used to determine nanoparticle size and

morphology of nanoparticles of all shapes. However, processing of the samples (e.g. under vacuum) might alter the properties of nanoparticles and, for organic nanomaterials, the electron density is often insufficient to allow direct detection by SEM or TEM without modification (63).

In addition to size and morphology, surface properties (e.g. surface charge and hydrophobicity) also play an important role in nanoparticle interaction with biological systems. Zeta potential (ζ-potential) provides indirect measurement of surface charge based on electrophoretic mobility (54). ζ-potential is defined as the difference of electro-kinetic potential on electrical double layer formed on particle surface and is closely linked to colloidal stability, especially for particles that rely on electrostatic repulsion to remain stable in dispersion (64). In these cases, a charge of ±30 mV is typically required to prevent aggregation. The effect of surface charge on nanoparticle-cell interaction has also been reported with positively-charged particles generally linked to increasing toxicity (65, 66).

Another interesting property of nanoparticles is the surface hydrophobicity. Although often overlooked, many have demonstrated the importance of this parameter on both the efficacy and safety of nanoparticles as drug carriers (30, 67, 68). Surface hydrophobicity has been related to the formation of the so-called 'protein corona' which can alter the distribution of nanoparticles in the body (69, 70). The assessment of surface hydrophobicity has historically relied on semi-quantitative or qualitative techniques such as dye partitioning, contact angle measurement, salt aggregation, and hydrophobic interaction chromatography (HIC) (68). The salt aggregation test (SAT) was initially developed to study the surface hydrophobicity of bacterial cells (71), while HIC is mostly used for protein purification. However, with some modifications HIC can be utilised to give more specific information on surface hydrophobicity based on the affinity of nanoparticles for different column beds (67).

This chapter will focus on the manufacture and characterisation of two types of nanomaterials: LNCs and PLGA-NPs. Both will be characterised, mostly to confirm particle size, narrow distribution and to investigate surface charge and hydrophobicity. Here, particular attention was given to the purification of the nanoformulations, mostly to remove excess stabiliser or surfactant, which could affect nanoparticle properties and behaviour (38, 43, 72).

## 2.2 Materials and methods

### 2.2.1 Materials

Labrafac™ Lipophile WL 1349 (medium-chain triglyceride (MCT) of caprylic [$C_8$] and capric [$C_{10}$] acids), Kolliphor® HS15 (PEG660-C18; 30% free PEG 660 and 70% PEG 660 hydroxystearate), and Lipoid® S75 (SPC; soybean phospholipid with 70% phosphatidylcholine) were kindly provided by Gattefosse (Saint-Priest, France), BASF SE (Ludwigshafen, Germany) and Lipoid GMBH (Ludwigshafen, Germany), respectively. Poly(D,L-lactide-co-glycolide) (PLGA; 75:25; molecular weight (mol. wt.) of 66,000-107,000), poloxamer 407 ($PEO_{98}$-$PPO_{67}$-$PEO_{98}$), sodium chloride (NaCl), ammonium thiocyanate ($NH_4SCN$) were purchased from Sigma-Aldrich (Gillingham, Dorset, UK). Kolliphor® P188 ($PEO_{52}$-$PPO_{30}$-$PEO_{52}$) was obtained from BASF (Ludwigshafen, Germany), ferric chloride anhydrous ($FeCl_3$) from Scientific Laboratory Supplies Ltd. (Wilford, Nottingham, UK), chloroform and acetone from Fisher Scientific Ltd. (Loughborough, Leicestershire, UK).

### 2.2.2 Methods

#### 2.2.2.1 Preparation and purification of lipid nanocapsules (LNCs)

LNCs were prepared using the phase-inversion method introduced by Heurtault *et al*. (37). The proportions of each material used are shown in Table 1 to produce three LNC formulations henceforth referred to as LNCX where X represents the intended diameter in nm. To make the LNCs, all the ingredients were dispersed in 3% w/w NaCl aq. and heated to 85 ºC under constant stirring. Then, the mixture was treated to three heating-cooling cycles (85 ºC–60 ºC–85 ºC–60 ºC–85 ºC). Following the last step, the emulsion was cooled down to 72 ºC at which point, cold water (4 ºC) was added to spontaneously form the nanosized particles. The amount of cold water added into the mixture was twice (LNC20 and LNC50) or 2.5-times (LNC100) the total weight of the emulsion. The LNCs were purified by dialysis (Float-A-Lyzer G2, UK; 300 kD MWCO) against deionised water (2 L); BioBeads® SM-2 (4 g) were added to aid in removing excess surfactant. During the dialysis process, the solvent and the beads were changed every hour for the first 3 hours, and then twice a day thereafter. LNC concentration was calculated based on the oil content from the initial formulation, thus the nanoparticle concentration for LNC50 and LNC100 were 56.67 mg/mL and 71.43 mg/mL, respectively.

**Table 1.** LNC composition[(1)]

| Formulation | Labrafac™ Lipophile WL1349 | Kolliphor® HS15 | Lipoid® S75 | NaCl aq 3%w/w |
|---|---|---|---|---|
| LNC20 | 8.25 | 25 | 1.75 | 65 |
| LNC50 | 17 | 17 | 1.75 | 64.25 |
| LNC100 | 25 | 8.5 | 1.5 | 65 |

[(1)]Proportion of LNC ingredients presented in %w/w

#### 2.2.2.2 Preparation and purification of PLGA nanoparticles (PLGA-NPs)

PLGA nanoparticles were prepared by a modified nanoprecipitation method (47). 100 mg of PLGA dissolved in 20 mL of acetone were added dropwise into 80 mL of a stabiliser solution. Two types of stabiliser materials (poloxamer 407, Kolliphor® P188) were tested at a concentration of 1% (w/v) and the formulations were then labelled as PLGA-P407 and PLGA-K188, respectively. The organic phase was then removed under constant stirring for 4 hours under the fume cupboard. Excess stabiliser was removed by washing the nanoparticles three times by centrifugation (9,000 g; 30 minutes). The nanoparticles were redispersed in distilled water and the final concentration was determined gravimetrically. The yield of the obtained nanoparticle was found to be ~28%, giving the final concentration of the nanoparticle suspension of ~1.4 mg/mL.

#### 2.2.2.3 Excess stabiliser assay

a) Sample preparation

For the LNCs, excess surfactant was separated from the particles by ultrafiltration (Amicon Ultra; 100 KDa MWCO; Millipore UK) at 13,000 g for 10 minutes. Meanwhile, for PLGA nanoparticles, samples were collected by pelleting down the nanoparticles (9,000 rpm; 15 minutes) and analysing the supernatant.

b) Assay procedure

The amount of surfactant remaining after purification was determined using a colorimetric method as previously described (73). Briefly, 50 μL of sample was added to 1.4 mL of a 50:50 mixture of chloroform and an aqueous chromophore solution (16.2 g/L $FeCl_3$; 30.4 g/L $NH_4SCN$). The biphasic mixture was stirred gently for 30 minutes at room

temperature. The lower chloroform layer was separated, and its absorbance measured ($\lambda_{max}$ = 510 nm) (Shimadzu UV-2600; Kyoto, Japan). The assay method was validated for individual stabilisers and calibration curves were obtained in triplicates (Table 2; Figure S1).

**Table 2.** Linear equation based on calibration curve of PEG-based surfactant spectrophotometry analysis

| Stabiliser | Linear equation[1] | Coefficient of determination ($R^2$)[1] | Linear range (mg)[2] | LoD (mg/mL)[2] | LoQ (mg/mL)[2] |
|---|---|---|---|---|---|
| Kolliphor® HS15 | y = 0.1302x + 0.1496 | 0.9960 | 0.1 – 2.5 | 0.211 | 0.641 |
| Poloxamer 407 | y = 0.3405x + 0.0881 | 0.9929 | 0.075 – 2 | 0.070 | 0.213 |
| Kolliphor® P 188 | y = 0.415x + 0.0359 | 0.9972 | 0.5 – 2 | 0.122 | 0.371 |

[1]Obtained from standard calibration curve from three independent measurements (*n*=3)
[2]Based on ICH guidelines of analytical method validation

### 2.2.2.4 Size and surface charge measurement

The size of nanoparticles was measured using dynamic light scattering (Malvern Nano-ZS, Malvern, UK). The measurements were carried out at 25 $^{o}$C at a 173$^{o}$ scattering angle. Refractive index (RI) for all samples was set at 1.590.

Zeta potential was measured based on the electrophoretic mobility of the particles in the dispersant using laser Doppler electrophoresis. The measurements were carried out at 25 $^{o}$C. For the measurements, the LNCs were diluted 1:50 in deionised water and 10 mM NaCl for size and zeta potential measurement, respectively. Meanwhile, PLGA nanoparticles were remained undiluted for both measurements.

### 2.2.2.5 Stability study of nanoparticles

Colloidal stability of nanoparticles stored 4 $^{o}$C was studied over time. Particle size and PdI were determined as described above, every week for 2 months. The stability of

nanoparticles in physiological condition was also assessed. Nanoparticles were dispersed in sterile phenol red-free cell culture media containing 10% foetal bovine serum and incubated at 37 $^{o}$C; particle size was recorded daily for 10 days. The nanoparticle-cell culture dispersion was prepared and incubated under sterile condition during the experiment.

#### 2.2.2.6 Assessment of nanoparticle surface hydrophobicity

a) Salt aggregation test (SAT)

This experiment was carried out by diluting the nanoparticles in aqueous NaCl solutions of varying concentration (0.5 M to 5 M). Aggregation was observed by following the change in size over time for 30 minutes at both 25 and 37 $^{o}$C. Measurements settings were adjusted to mimic the changes in RI and viscosity of the dispersing medium at increasing salt concentrations.

b) Hydrophobic interaction chromatography (HIC)

The surface hydrophobicity of nanoparticles was assessed based on the surface affinity into hydrophobic interaction column, namely butyl, phenyl, and octyl. Briefly, 100 µL of nanoparticle suspension in PBS (5 mg/mL for LNCs and ~1 mg/mL for PLGA-NPs) were introduced in the column and eluted, first with 10 ml PBS, followed by 15 mL of Triton X-100 (0.5% w/v). 1 mL fractions were collected for both eluents and analysed based on turbidity ($\lambda$max = 450 nm) (Fluostar Omega, BMG Labtech). The absorbance values were plotted against the volume and the AUCs of the resulting peaks were determined for each eluent. The particle retention in each of three columns was determined by following (67):

$$\% \text{ column retention } (\%R) = \left(\frac{\text{AUC TritonX}}{\text{AUC PBS + AUC TritonX}}\right) x\ 100 \qquad \text{Eq. 1}$$

The HIC index value was calculated according to the equation (67):

$$\text{HIC Index} = \frac{(\%R_{butyl} \times \log P_{butyl}) + (\%R_{phenyl} \times \log P_{phenyl}) + (\%R_{octyl} \times \log P_{octyl})}{(100\% \times \log P_{butyl}) + (100\% \times \log P_{phenyl}) + (100\% \times \log P_{octyl})} \quad \text{Eq. 2}$$

whereby, logP values of each column were stated as: 0.47, 0.94, and 2.05 for butyl, phenyl, and octyl, respectively (67). Meanwhile, for the denominator, each logP value was multiplied by 100% representing the condition of 100% retention.

#### 2.2.2.7 Statistical analysis

Data calculation, graphs processing and statistical analysis were carried out using GraphPad Prism Software (California, USA). For paired data, statistical analysis was carried out using Student's t-test. Meanwhile, for groups of data, one-way ANOVA and post-hoc Dunnett's test for multiple comparisons were used.

## 2.3 Results and discussion

### 2.3.1 Manufacture and characterisation of LNCs

LNCs were prepared successfully using the phase-inversion method. This method involves several heating-cooling cycles followed by sudden temperature drop to form the nanostructure (37). During the temperature cycling, the type of emulsion changes from oil-in-water (low temperatures) to water-in-oil (>85 $^{o}$C) as a result of the change in the hydration of the PEGylated surfactant with temperature (38). At the end of the last cycle, when the temperature reaches 72 $^{o}$C, the mixture exists as a microemulsion and the addition of cold water allows the formation of nanocapsules with well-defined properties. The size of nanocapsules can be controlled by varying the composition of the LNCs. Of all the ingredient, the oil (Labrafac® Lipophile WL 1349) and the surfactant (Kolliphor® HS15) play the most

significant role in determining particle size. As expected, a higher oil proportion will lead to larger particle size, while a higher surfactant content will stabilise the system, forming smaller particles (37, 38).

In this study, LNCs with three different sizes were prepared: 20, 50, and 100 nm. The obtained particle size for the three formulations agreed with predicted sizes. This suggests that it is possible to control the size of the nanoparticle formulation by varying the ingredient proportion based on the ternary diagram proposed by Heurtault *et al*. (38).

Following the preparation, the LNCs were purified by dialysis. The aim of purification is to remove excess surfactant that may possess its own toxicity (43). Because of the nature and size of LNCs, purification through centrifugation is not feasible due to the risk of destabilising. Here, LNC purification was carried out using a membrane with a 300 kDa molecular cut-off. In a study conducted by Vonarbourg *et al*. (41) a 30% reduction in the concentration of free surfactant could be achieved after 48 hours of dialysis against deionised water, using a 50 kDa membrane. The study was carried out on three different sizes of LNCs as well, 20 nm, 50 nm, and 150 nm, and there was no difference observed regarding the percentage of surfactant removed following the dialysis.

It was expected that by using membrane with higher molecular cut-off, maximum removal could be achieved because of the larger pore size. Here, despite using a membrane with a 6-times higher MWCO, only a small proportion of the surfactant was removed after 3 days, when dialysed against water. Consequently, a modified resin adsorbent (BioBeads® SM-2 Resin) was also added to the water to help the removal process. As the dialysis depends on osmosis, the addition of this adsorbent will help to entrap the surfactant molecule in the dialysis media, thus increasing the transfer of the surfactant across the membrane. Previously, Jones *et al*. (67) had successfully demonstrated that this method could be used to bring the free surfactant

concentration to <0.5 mg/mL in 72-hours. However, longer durations were required in the present study to achieve similar results. Indeed, after 72-hours of dialysis, the content of remaining surfactant for both formulations was still very high (data are not shown). Thus, further optimisation by daily sampling was required. The maximum removal of excess surfactant (surfactant concentration <LoQ) was obtainable after 7 days of dialysis for LNC50 and 4 days for LNC100. Meanwhile, for LNC20, after 9 days of dialysis, the measured surfactant content was still very high (~3.2 mg/mL). In correlation with the toxic effect of the surfactant used which will be discussed in the next chapter, LNC20 was excluded from further studies.

The properties of LNCs before and after purification are summarised in Table 3. The characterisation of the LNC formulations before purification showed that the three formulations met the intended size with measured hydrodynamic diameter of 23.4 ± 2.0 nm, 45.6 ± 1.9 nm, and 109.9 ± 3.4 nm for LNC20, LNC50, and LNC100, respectively. Results have shown that there is no significant difference between the purified and non-purified LNC50 and LNC100 in terms of the particle size. There was no variation between batches of LNCs, suggesting that the preparation method used is reproducible. The PdI for both LNCs ranged between 0.05 – 0.11 which indicates the obtained nanocapsules have a narrow size distribution (PdI <0.3). The uniformity of particle size is one of important factors in nanoparticle preparations as it has a great influence on the formulations (stability, drug loading, entrapment efficiency) and the fate of nanoparticles *in vivo* (74). The surface charge of LNCs was found to be slightly negative to neutral which is in agreement to the published values for LNC50 and LNC100 before and after purification (39, 75).

**Table 3**. Properties of LNCs before and after purification[(1)]

| Parameter | Before purification | | | After purification[(2)] | | |
|---|---|---|---|---|---|---|
| | **LNC20** | **LNC50** | **LNC100** | **LNC20** | **LNC50** | **LNC100** |
| **Hydrodynamic diameter (nm)** | 23 ± 2 | 46 ± 2 | 110 ± 3 | n/e | 44 ± 2 | 109 ± 5 |
| **PdI** | 0.13 ± 0.07 | 0.11 ± 0.04 | 0.05 ± 0.03 | n/e | 0.10 ± 0.06 | 0.08 ± 0.02 |
| **ζ-potential (mV)** | −7 ± 2 | −7 ± 3 | −8 ± 1 | n/e | −9 ± 1 | −8 ± 2 |
| **Theoretical surfactant concentration (mg/mL)** | 83 | 57 | 24 | - | - | - |
| **Actual surfactant concentration (mg/mL)** | n/e | 53 ± 4 | 24 ± 1 | ~3 | <LoQ | <LoQ |

[(1)]Data are presented as mean ± SD from three individual batches ($n$=3); n/e = not evaluated
[(2)]Statistical analysis using t-test found no significant difference in hydrodynamic diameter, PdI, and ζ-potential of LNC50 and LNC100 before and after purification

Colloidal stability of LNCs in this study was assessed over two months. This stability test was only conducted on the purified LNCs. Figure 7a and 7b confirmed that both LNC50 and LNC100 showed excellent stability at storage (4 $^{o}$C). This agrees with previous finding stating that LNCs are stable at 4 $^{o}$C for up to 18 months (37). Here, colloidal stability at room temperature was not tested, but previous reports have demonstrated that LNC formulations were stable at 25 $^{o}$C and even at higher temperature (37 – 40 $^{o}$C) (37, 67, 76). At 37 $^{o}$C, LNCs remained stable for 1.5 months (37). The physical stability of LNCs is obtained not only from the steric stabilisation provided by the PEG, but also from the semi-rigid shell composed of PEG-stearate and SPC, preventing the oily core from coalescence (38). At room temperature and below, the extended stability of LNCs is expected to result from the fact that the PEG-stearate in the capsule shell solidifies (36, 76).

The stability of LNCs was also observed under physiological conditions which were reproduced *in vitro* by dispersing the nanoparticles in cell culture media supplemented with 10% foetal bovine serum. Results showed that the LNCs were relatively stable for 10 days (Figure 7c and 7d). A change in PdI was observed for both LNC50 and LNC100 during the study period. However, the values remained within the acceptable range (<0.3). This suggests that there may be an interaction between the nanocapsules and a component of culture media, e. g. serum (70).

To summarise, LNCs prepared with phase-inversion method in this study exhibited excellent physicochemical characteristics and stability. However, as the preparation method involves high temperatures, this particular type of nanoparticle may not be suitable for thermosensitive drugs (e.g. vaccines and hormones). On the other hand, the long purification process may become an additional drawback. Here, biodegradable PLGA-NPs were prepared for comparison and as a possible alternative.

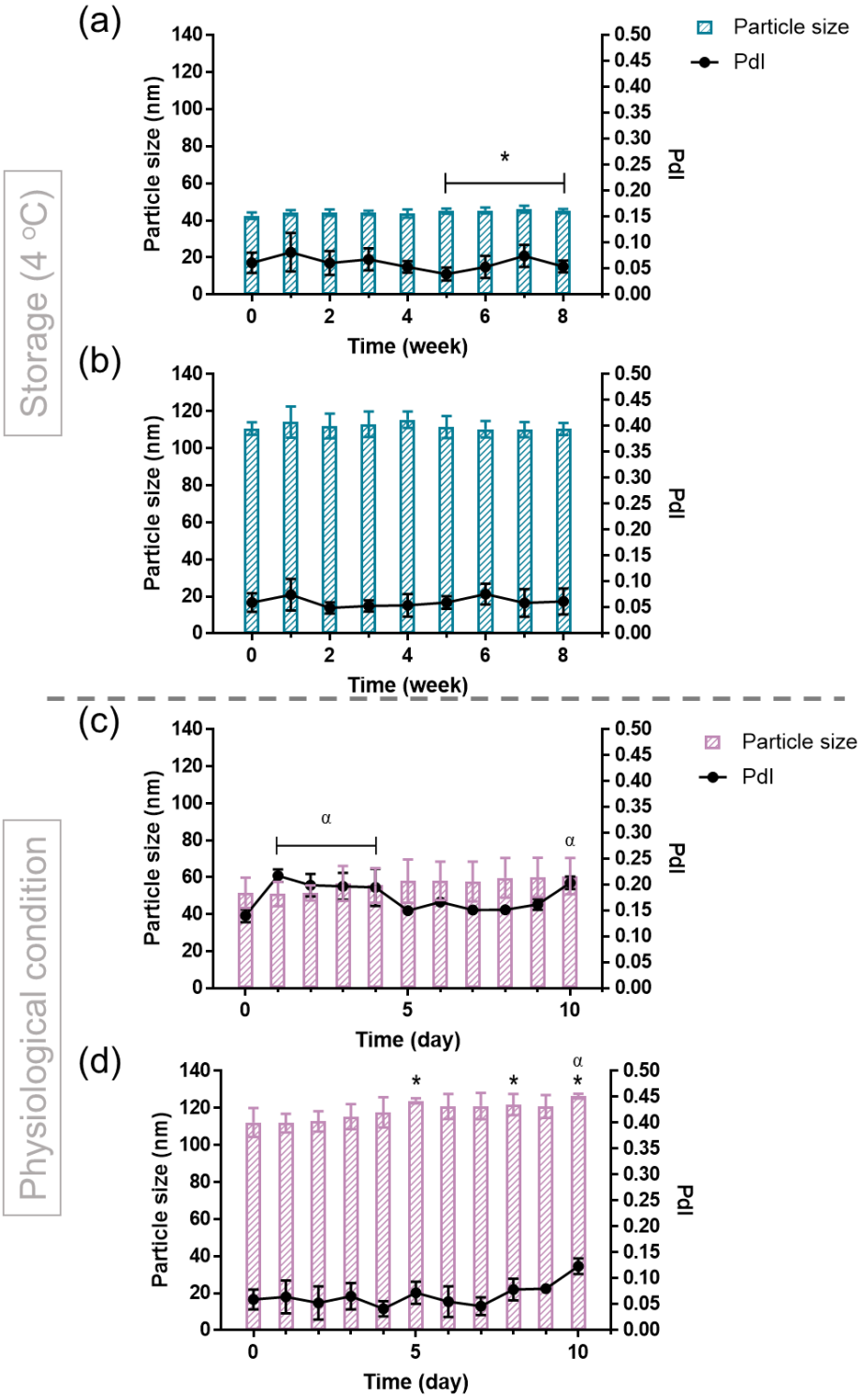


**Figure 7.** Colloidal stability of LNC formulations at storage 4 °C ((a) = LNC50; (b) = LNC100) and in physiological condition ((c) = LNC50; (d) = LNC100). Data presented as mean ± SD from three individual batches ($n$=3). Statistical analysis using one-way ANOVA for particle size* and PdI$^{\alpha}$ ($p<0.05$), compared to the initial measurement (week/day = 0).

### 2.3.2 Manufacture and characterisation of PLGA-NPs

PLGA-NPs were prepared using nanoprecipitation or solvent-evaporation method. Poyvinyl alcohol (PVA) is the most commonly used stabiliser for these types of nanoparticles. However, compatibility issues have been reported as PVA coating may not hinder the protein absorption on nanoparticle surface (77). Poloxamer-based surfactants have been proposed as an alternative (51). In this study, poloxamer 407 and Kolliphor® P188 were used as stabilisers for the PLGA-NPs. Poloxamer-based surfactants have been used extensively in pharmaceutical technology because of their excellent properties and biocompatibility. Poloxamer is a non-ionic triblock copolymer, consisting of hydrophobic polypropylene oxide (PPO) and hydrophilic polyethylene oxide (PEO) chains. Different types of poloxamer are obtainable depending on the number of units in each moiety. PPO acts as the central chain, flanked by two PEO chains. The number of EO/PO/EO units in Poloxamer 407 and Kolliphor® P188 are 98/67/98 and 52/30/52, respectively (78).

Previous studies suggested that there should be no difference in size for PLGA-NPs obtained from these two stabilisers (51) which was confirmed here (Table 4). Both formulations exhibited narrow size distributions with PdI <0.1. Surface charge for both nanoparticle preparations was negative with ζ-potential value of −36.7 ± 0.8 and −32.1 ± 3.7 mV for PLGA-P407 and PLGA-K188, respectively. This negative charge is caused by the presence of ionized carboxyl groups, from the polymer chains, on the nanoparticle's surface. Numerous studies have demonstrated that the zeta potential of nanoparticles prepared from PLGA only have zeta potential closer to −40 mV. Because of the stabiliser coating, the surface charge PLGA-NPs in this study were slightly lower. It is suggested that the coating masks the surface charge, thus reducing the zeta potential (51, 79).

**Table 4.** Properties of PLGA-NPs[(1)]

| Particles | Hydrodynamic diameter (nm) | PdI | ζ-potential (mV) |
|---|---|---|---|
| PLGA-P407 | 179.2 ± 4.2 | 0.09 ± 0.066 | −36.7 ± 0.8 |
| PLGA-K188 | 162.1 ± 1.0 | 0.08 ± 0.018 | −32.1 ± 3.7 |

[(1)]Data are presented as mean ± SD from three individual batches ($n$=3)
[(2)]Statistical analysis using *t-test* found no significant difference in hydrodynamic diameter, PdI, and ζ-potential between different stabilisers used

As polyester-based nanomaterials, PLGA-NPs are susceptible to degradation in aqueous media Thus, it is important to assess the stability of the nanoparticle suspension over time to observe any reduction in particle size which may indicate that degradation had taken place. Previous studies have shown that one of the factors affecting the degradation rate is the ratio of lactic acid (LA) and glycolic acid (GA) composing the polymer, with the former being more hydrophobic than the latter (46). LA is known to be hydrophobic while GA is hydrophilic, thus higher LA content will prevent the access of water to the polymer backbone. Degradation of PLGA polymer may occur in four steps: hydration, initial degradation, constant degradation, and solubilisation (80). Here, the LA:GA ratio of PLGA polymer used in the preparation was 75:25. A study conducted by Wu and Wang (46) has found that the PLGA polymer with this ratio exhibited ~50% of degradation after 20 days when dispersed in PBS (pH 7.4) at 37 $^{o}$C under constant stirring. Additionally, Dong *et al*. (81) demonstrated that degradation of PLGA in water is more likely to occur at higher temperature near or above the glass transition temperature of the polymer (Tg = ~45 $^{o}$C). As expected, nanoparticles produced from PLGA (75:25 LA:GA) had excellent storage stability (4 $^{o}$C) suggesting minimal degradation or aggregation (Figure 8a and 8b). The lack of aggregation likely results from steric repulsion

afforded by polymer coating on the nanoparticle surface as well as electrostatic repulsion between the negatively charged particles (51, 78, 82).

In comparison, changes in the particle properties was observed under physiological conditions (Figure 8c and 8d). Indeed, the size of PLGA-K188 NPs was seen to increase on day 6, though no further increases were noted until the end of the experiment; PLGA-P407, however, did not experience any change in size until day 9. Interestingly, the PdI increased over time for PLGA-P407 (ca. ~2.5-fold increase between days 0 and 10), but not for PLGA-K188. The complexity of the composition of cell culture medium (e.g. salts, serum) is likely to have contributed to this phenomenon. These findings altogether suggest that both formulations exhibited some changes under physiological condition, despite the difference stabilisers used during preparation. This is in agreement with the finding Oliveira *et al*. (83) wherein it was demonstrated that the interaction between PLGA-NPs with protein is independent to the surface properties.

Comparing both types of nanoparticles, it appears that only LNC100 were completely stable (no change in size or PdI), while LNC50, PLGA-407, and PLGA-K188 all experienced some change, although this was not necessarily significant. This may be related to the surface hydrophobicity of the nanoparticles which will be elaborated in the next section.

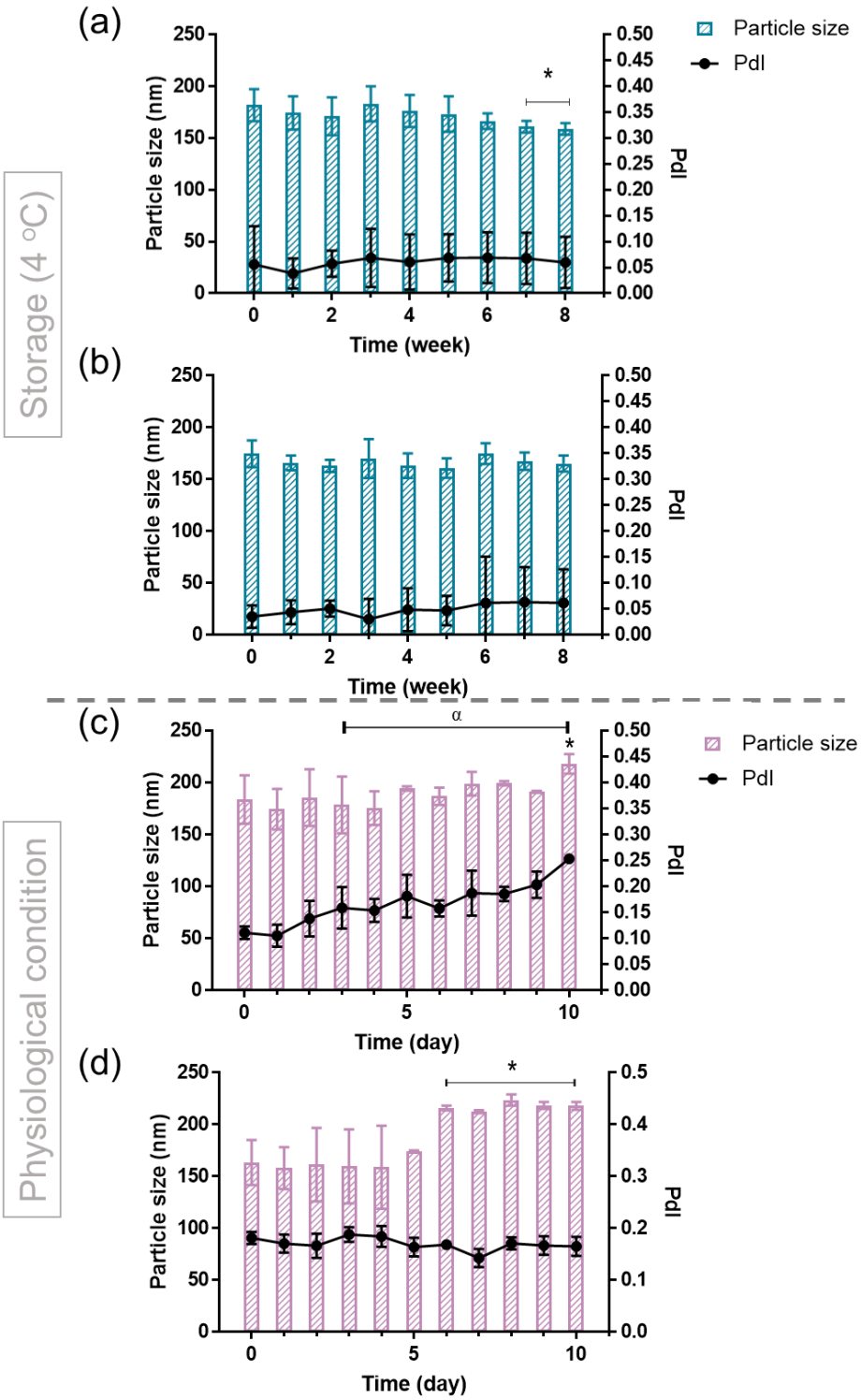


**Figure 8.** Colloidal stability of PLGA-NPs formulations at storage 4 °C ((a) = PLGA-P407; (b) = PLGA-K188) and in physiological condition ((c) = PLGA-P407; (d) = PLGA-K188). Data presented as mean ± SD from three individual batches ($n$=3). Statistical analysis using one-way ANOVA for particle size* and PdI$^{\alpha}$ ($p<0.05$), compared to the initial measurement (week/day = 0).

### 2.3.3 Assessment of nanoparticle surface hydrophobicity

Besides particle size and surface charge, another interesting property of nanoparticles that could be analysed is surface hydrophobicity. Surface hydrophobicity has been reported to be related to the fate of the nanoparticle inside the body, for example the formation of nanoparticle-protein corona (70). There are numerous methods to assess surface hydrophobicity of nanoparticles, either qualitatively or quantitatively (67, 68). The first method used in this study is SAT (71). The test is based on the salting-out phenomenon wherein the sample is diluted in salt solution of increasing concentrations. The more hydrophobic the nanoparticle surface, the more likely it is that aggregation will occur as the presence of salts disturbs the fragile thermodynamic equilibrium (84). Here, NaClaq was used at concentration between 0.5 – 5 M and the change in particle size was measured along time for 30 minutes at two different temperatures, 25 and 37 $^{o}$C.

Because of their higher surfactant content, it was hypothesised that LNC50 would have a more hydrophilic surface compared to LNC100. However, the results suggest the contrary. No evidence of aggregation was seen for either LNCs at 25 $^{o}$C, even at the highest salt concentration. Meanwhile, at 37 $^{o}$C, higher extent of aggregation was observed for LNC50, but not LNC100, where the final size of LNC50 at 5 M NaCl increased ~26.6-fold (Figure 9).

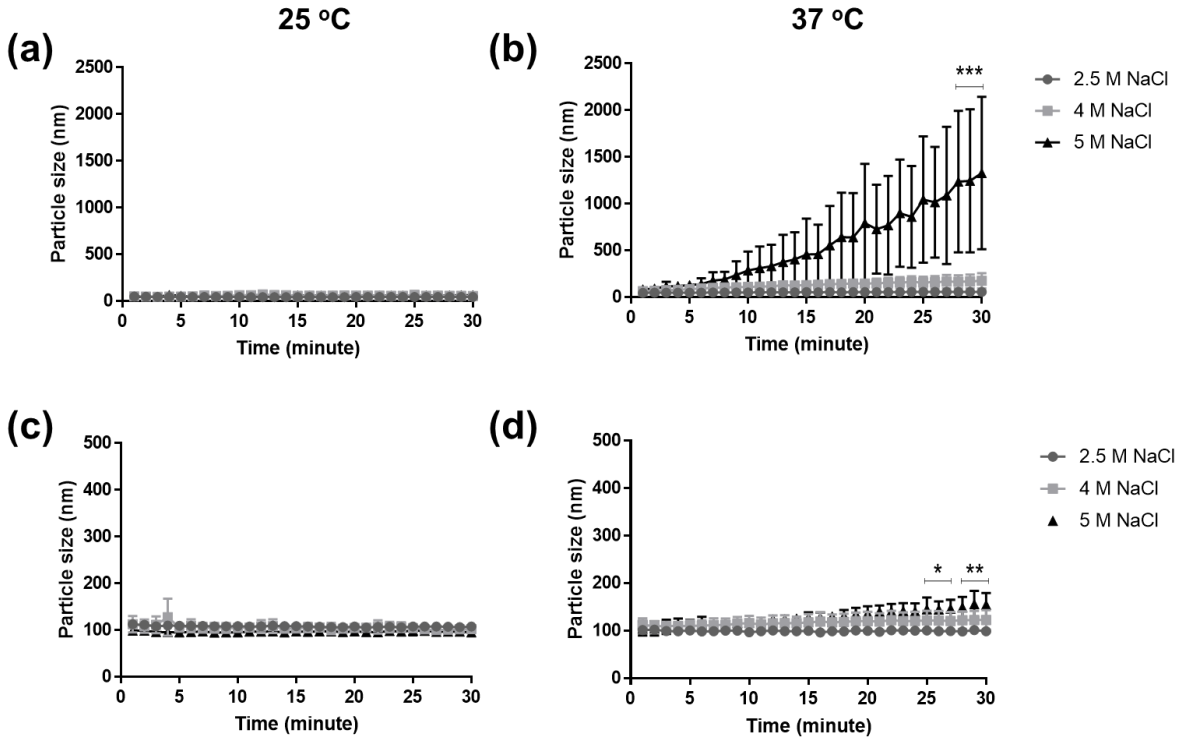


**Figure 9**. Salt aggregation test of LNC50 (a,b) and LNC100 (c,d) at 25 and 37 °C. Data are presented as mean ± SD from three individual batches (*n*=3). Statistical analysis using one-way ANOVA compared to the initial particle size (min = 0) measured under the same condition, **p<0.05, **p<0.01, ***p<0.001*.

The main surfactant used for LNC preparation consists of a mixture of free PEG chains, oriented to water, and HS-PEG (hydroxystearate PEG) chains, oriented to the oily core of LNCs. The arrangement of these PEG chains on the surface can determine the interaction between the nanocapsule surface and its surrounding environment (41). For LNC50, it is possible that the higher surfactant concentrations during preparation led to a disordered arrangement (Figure 10a). This structure causes the surface to become less hydrated due to the exposure of the hydrophobic HS-PEG chains that are loosely attached on the nanocapsule surface (41, 85). For LNC100, because of the initially lower surfactant concentration, the PEG chains configure in a more ordered arrangement (Figure 10b) allowing better hydration of the hydrophilic portion (41, 86).

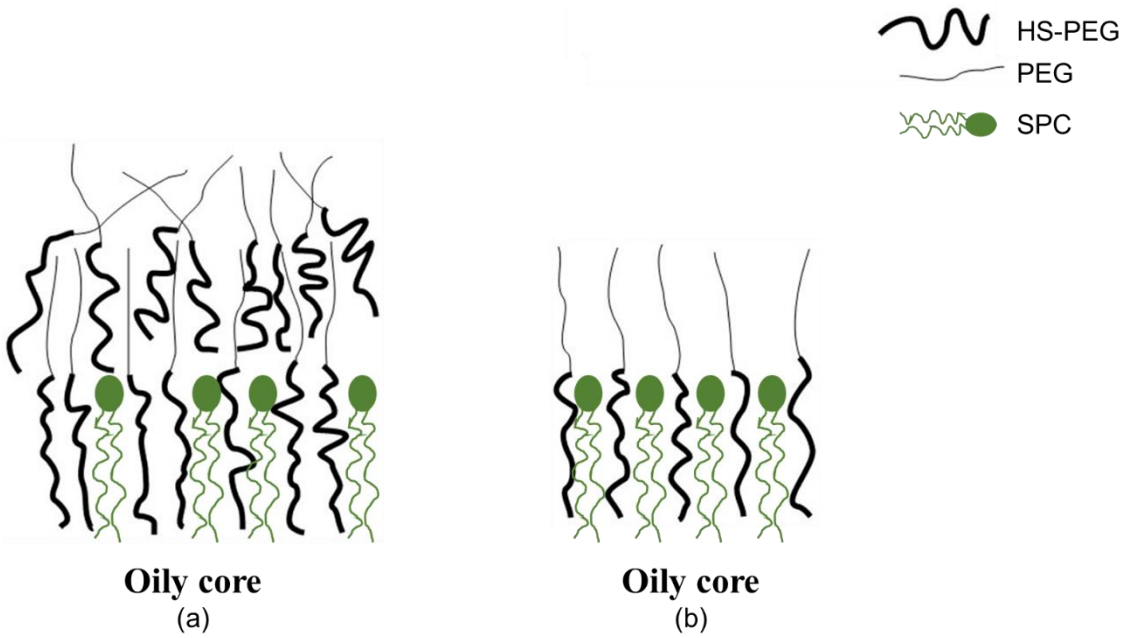


**Figure 10**. Schematic representation of PEG configurations on LNC surface in (a) disordered and (b) ordered arrangements; adapted and modified from Vonarbourg *et al*. (41)

Although the dialysis process had removed a significant amount of surfactant, the hypothesis is there are still enough surfactant molecules to form a dense layer on LNC50 surface. This condition may be more susceptible to change in hydration due to increasing salt concentration. Indeed, high salt concentration will influence the hydration status of the nanocapsule surface due to the increase of ion-water interaction (87). The effect of temperature on aggregation was clearly shown since aggregation only occurred at 37 $^{o}$C. At higher temperature, the ion-water interaction becomes stronger. Consequently, salting-out is more likely to occur (87). However, as the extent of aggregation is different between the two LNCs, it is suggested that the change of electrolyte-water bond at high concentration and/or temperature contribute rather smaller impact compared to the arrangement of the HS-PEG chains on the surface (41).

The SAT was also carried out on PLGA-NPs and the results are presented in Figure 11. In contrast to LNCs, where no aggregation occurred at 25 $^{o}$C, both PLGA-NP formulations aggregated at room temperature, although only to a very small extent. At 37 $^{o}$C, both formulations exhibited a change in size in a salt concentration-dependent manner; where PLGA-P407's size increased ~8-fold at 5 M NaCl. Aggregation could be seen for both particles in a 2.5 M salt solution, where PLGA-K188 aggregate to a size ~2.2x bigger than PLGA-P407 after 30 minutes. The slight differences in the behaviour of both formulations in concentrated salt solutions can be explained by the arrangement of surfactant on the nanoparticles' surface. The central part of this surfactant type is composed of the polypropylene oxide (PPO) segment which, in principle, will bind to the surface through hydrophobic interactions. For that reason, the PPO blocks are also called "anchor" blocks. Meanwhile, the more hydrophilic polyethylene oxide (PEO) chain will orientate itself towards the aqueous medium forming what is called the "buoy" blocks. The packing and attachment of the triblock copolymer on the surface of the nanoparticles depend mostly on the length of PPO chain (50, 88). However, other factors such as the nature of the core polymer and the surfactant itself may influence the surface coverage (72). Shorter PPO block of Kolliphor® P188 leads to lesser hydrophobicity of the surfactant compared to poloxamer 407. For that reason, it is hypothesised that the attachment of Kolliphor® P188 onto PLGA-NP surface is weaker and may leave more of the hydrophobic PLGA core exposed.

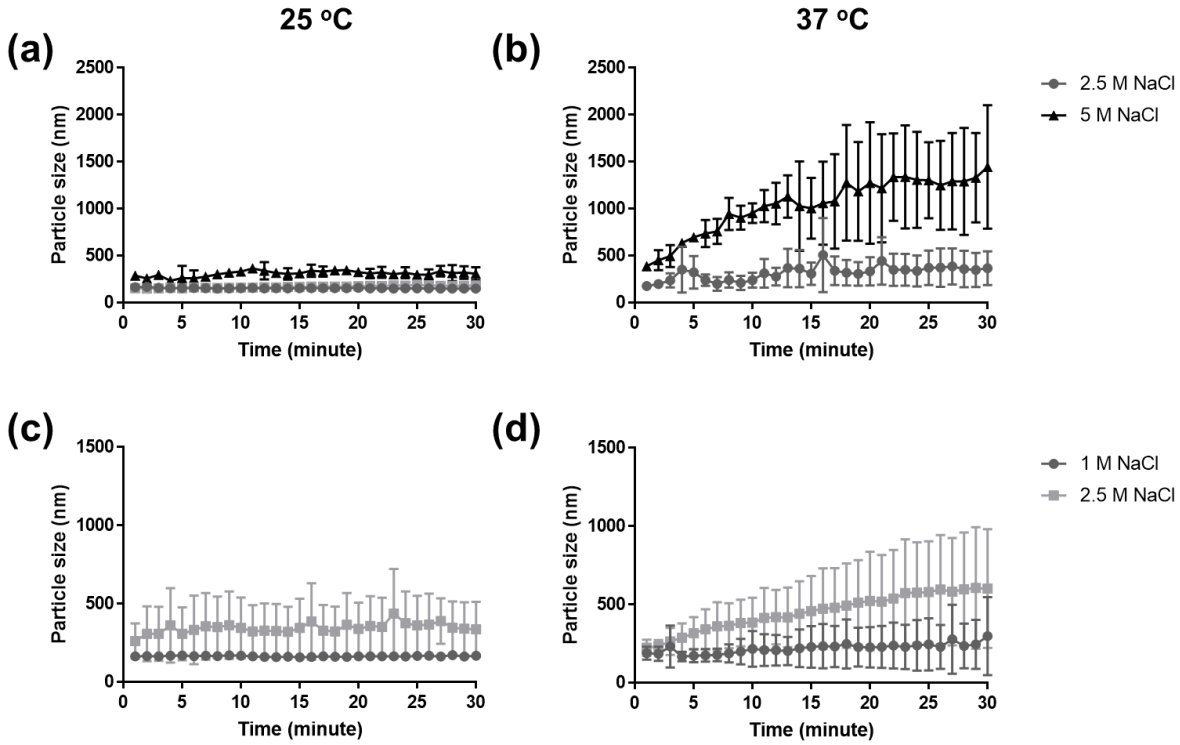


**Figure 11**. Salt aggregation test of PLGA-P407 (a,b) and PLGA-K188 (c,d) at 25 and 37 °C. Data are presented as mean ± SD from three individual batches (*n*=3). Statistical analysis using one-way ANOVA compared to the initial particle size (min = 0) measured under the same condition, no significant difference was found in the size increase over time.

Surface hydrophobicity of LNCs and PLGA-NPs was also determined using HIC. Using the % retention for the nanoparticles on HIC column of differing hydrophobicities, an HIC index ranging between 0 – 1, where 0 is extremely hydrophilic and 1 is extremely hydrophobic, was calculated (67). The HIC indices of LNC100 and LNC50 were 0.55 ± 0.08 and 0.50 ± 0.10, respectively (*p=0.8637*). Those values showed that both LNCs are considered to be hydrophilic (HIC index <0.7). In comparison, the HIC indices of PLGA-P407 and PLGA-K188 were 0.78 ± 0.07 and 0.83 ± 0.08, respectively, suggesting the more hydrophobic surface compared to LNCs.

The difference between LNCs and PLGA-NPs in general agreed with the results obtained from the SAT wherein LNCs generally appeared to be less hydrophobic than PLGA-NPs. The slight, non-significant, difference between PLGA-P407 and PLGA-K188 (*p=0.8263*) also

agreed with the SAT result where PLGA-K188 had a stronger tendency to aggregate, even at room temperature. However, the mean HIC index values for the LNCs indicated that LNC100 were slightly more hydrophobic, though again, this was not significant. Altogether, both SAT and HIC experiments showed that PLGA-NPs are more hydrophobic than LNCs. As discussed above this is likely due to differences in the stabiliser used and its arrangement on the particle's surface. It could be argued that the validity of HIC as a method to estimate hydrophobicity is not physiologically-relevant as the experiment is carried out at room temperature in the presence of low salt concentration, where no significant change in surface hydration is likely to occur. Yet, and importantly, the method was able to detect small differences in surface hydrophobicity that would not have been detected in a SAT carried out at 25 $^{o}$C at the same ionic strength.

The HIC index obtained from this experiment can be used as a predictor of *in vivo* effect of the nanoparticles, such as immune response activation as demonstrated by Jones, *et al*. (67) It was found that polystyrene (PS) and polyvinyl acetate (PVAc) nanoparticles with HIC index >0.8 triggered immune response in the respiratory system, while LNCs with HIC index <0.7 showed very little impact. Compared to the result obtained in this study, it is suggested that LNCs are more biocompatible compared to PLGA-NPs, although further assessment is imperatively required.

## 2.4 Conclusion

LNCs and PLGA-NPs with a narrow distribution were successfully manufactured. Both nanoparticles were stable at 4 $^{o}$C and physiological condition, even following the removal of excess stabiliser. For PLGA-NP, no significant difference in terms of particle size and surface charge between PLGA-P407 and PLGA-K188 were observed. Salt aggregation test (SAT) and

hydrophobic interaction chromatography (HIC) were used to assess the surface hydrophobicity. Overall, the results from these studies generally suggested that PLGA-NPs were more hydrophobic than LNCs. Carrying the SAT at physiological temperature further revealed interesting patterns which could be linked to differences in the conformation of the stabiliser on the particle's surface. It remains to be seen what impact these small differences will have on the fate of the nanoparticles following nose-to-brain administration.

# 3. Cell study

## 3.1 Introduction

Nanoparticulate delivery system for nose-to-brain delivery is a strategic approach to efficiently transport drug molecules to the CNS. Compared to free drugs, nanoparticles provide several advantages, i.e. increase organ targeting capability (10). However, despite the benefits, the toxicological aspect of nanoparticles must be taken into account during the formulation process. Several factors, such as chemical composition, particle size and shape, surface properties of nanoparticles can help to predict both the efficacy as drug carrier system and potentially harmful effects. Thus, although generally considered to be biocompatible, the assessment of the toxicity of organic nanoparticles remains an important part of the characterisation studies (30). As previously explained, in nose-to-brain delivery, drugs or other molecules are transported either intracellularly from the nerve endings or extracellularly along the ensheathing channels to reach the brain tissues (13). As interaction with neurons cannot be avoided, it is important to assess the compatibility of nanoparticles formulated for nose-to-brain delivery with neuronal cells (89). To this end, SH-SY5Y neuroblastoma cells were used as a model in this study.

SH-SY5Y were originally derived from the parental SK-N-SH cell line and are often utilised in neurobiology-related studies to avoid the limitations of primary neurons. The drawbacks of using primary neurons include high cost during preparation and lack of cell division following terminal differentiation (90). Moreover, numerous studies have used undifferentiated SH-SY5Y in preliminary studies with the aim to predict the effect of nanoparticles into neuronal cells (91-93). The current study will focus on two specific types of nanoparticles. First, lipid nanocapsules (LNCs) are great candidates as nanocarriers for nose-to-brain delivery due to their biocompatibility and ability to enhance drug transport through

biological membrane (35). However, Maupas, *et al*. (43) reported that surfactant-dependent cytotoxicity might occur following LNCs exposure; a result that was confirmed in another study (42). Specifically, the surfactant, PEG-C18 is linked to toxicity due to its ability to cause disruption of cell membrane. In contrast, PLGA nanoparticles (PLGA-NPs) do not generally suffer from this issue since the preparation process does not require high concentrations of stabiliser as seen for LNCs. However, for polymeric nanoparticles, stability and aggregation under physiological conditions may be more problematic which is due to the hydrophobic nature of the polymer itself (94).

*In vitro* toxicity assays based on metabolic dyes such as tetrazolium salt (e.g. MTT) are still the first choice if a simple and reliable method to determine cell viability is needed (95). These assays exploit the mitochondrial activity of healthy cells to convert the water-soluble yellow tetrazolium compound into insoluble purple formazan crystal. The obtained formazan crystals are then solubilised using solvent such as dimethyl sulfoxide (DMSO) before determining the absorbance of resulting solution using a spectrophotometer. Nowadays, other dyes with similar properties can be found, namely XTT and MTS assay. The use of the latter water-soluble dyes will eliminate the need for a solubilising step. However, not all cell types are suitable for these assays and the MTT assay is reported to be the more robust method in assessing cell viability in most cell lines (96).

In addition to cytotoxicity, the cellular uptake of nanoparticles is another important point to be assessed. Common pathways leading to nanoparticle internalisation into non-phagocytic cells include clathrin-mediated endocytosis, caveolae-dependent endocytosis, clathrin/caveolae-independent endocytosis, macropinocytosis, and receptor-mediated endocytosis (97). For neuronal cells, caveolae-dependent endocytosis hardly exists because this type of cell lacks the caveolin protein (23). Most methods to study uptake rely on the detection

of fluorescently-labelled nanoparticles and fluorescent dyes, such as nile red, can be incorporated into nanoparticles during preparation allowing uptake to be tracked by fluorescence microscopy or flow cytometry (98). The main advantage of flow cytometry is to provide the ability to collect information from thousands of cells per second for rapid analysis (99, 100). Moreover, it is now possible to observe the specific pathway of nanoparticle uptake into the cells by using a pharmacological inhibitor that selectively perturbs different endocytic mechanisms (101). Altogether, the results from these experiments will provide us with a better understanding of interactions between nanoparticles and cells which is beneficial to predict the fate of nanoparticles *in vivo*.

## 3.2 Materials and methods

### 3.2.1 Materials

Dulbecco's Modified Eagle Medium/ Nutrient Mixture F-12 (DMEM/F12) (1:1), Dulbecco's phosphate buffered saline (DPBS), penicillin-streptomycin (10,000 U/mL), heat-inactivated foetal bovine serum (HI FBS), 0.25% trypsin-EDTA, and nile red were purchased from Fisher Scientific Ltd. (Loughborough, Leicestershire, UK). Thiazolyl blue tetrazolium bromide (MTT powder), chlorpromazine hydrochloride, and triton X-100 were obtained from Sigma-Aldrich (Gillingham, Dorset, UK).

### 3.2.2 Methods

#### 3.2.2.1 Cell culture

SH-SY5Y cells were cultured in DMEM/F-12 (1:1) with L-glutamine supplemented with 10% foetal bovine serum and 1% penicillin/streptomycin (500 U/mL) and kept at 37 $^{o}$C

and 5% $CO_2$. The culture was passaged when it reached ~80% confluency using 0.25% trypsin-EDTA (5). The passage number of the cells used was 1 to 18.

### 3.2.2.2 Cytotoxicity assay

The cytotoxicity of the nanoparticles and surfactants used in this study was assessed based on mitochondrial activity of the cells (102). The cells were plated into 96-wells plate at a density of 1 x $10^4$ cells/well and allowed to attach for 24 h. The cells were then treated with varying concentrations of the material (surfactants or nanoparticles) for 1 to 72 hours. The particle concentrations used were 0.01 – 5 mg/mL and 0.0025 – 1.4 mg/mL for LNCs and PLGA-NPs, respectively.

Following treatment, the cells were washed using DPBS and replenished with 90 μL fresh medium with 10% FBS. 10 μL of 5 mg/mL MTT solution was added into each well and the plates were incubated at 37 ºC for 2 hours. Then, the supernatant was carefully removed and 100 μL DMSO was added into each well to dissolve the formazan crystals. The plates were left incubated for another 10 minutes at 37 ºC. The absorbance was measured using plate reader (Fluostar Omega, BMG Labtech, Aylesbury, UK) at λ=570 nm. The % of cell viability was calculated using Eq. 3:

$$\% \text{ cell viability} = \frac{(\mathrm{OD}_{\text{treatment}} - \mathrm{OD}_{\text{positive control}})}{(\mathrm{OD}_{\text{untreated}} - \mathrm{OD}_{\text{positive control}})} \times 100\% \qquad \text{Eq. 3}$$

where OD = optical density obtained from absorbance value recorded in the instrument.

### 3.2.2.3 Incorporation of nile red fluorescent dye into nanoparticles

Fluorescently-labeled LNCs and PLGA-NPs were prepared using methods described in the previous chapter (Method 2.2.2.1 and 2.2.2.2). For the LNCs, nile red was dissolved in the

oil (Labrafac™ Lipophile WL 1349) to form 0.025% w/w solution. Meanwhile, for the PLGA-NPs, 0.01% w/v nile red in acetone was prepared and further used as the organic phase for the nanoparticle preparation.

#### 3.2.2.4 Cellular uptake analysis

a) Flow cytometry

SH-SY5Y cells were plated at density of 0.2 x $10^6$ cells/well in 12-well plate. The cells were then incubated with nile red-loaded LNCs (0.16 – 0.62 mg/mL) and PLGA-NPs (0.08 – 0.35 mg/mL) for selected time points (2-hour for kinetic study and 24-hour for longer exposure uptake) . Cells were then washed with DPBS and detached with 0.25% trypsin-EDTA. The cells were collected by centrifugation (200 g, 5 minutes) and re-dispersed in 500 μL cold DPBS. The samples were kept on ice prior to analysis on a flow cytometer (BD LSRFortessa, BD Biosciences). The fluorescence was detected using excitation laser line (Ex) = 488 nm and emission (Em) = 613 nm. A total of 10,000 events were collected for each specimen.

b) Fluorescence microscopy

The cells were plated under the same condition as with the flow cytometry analysis above and treated with the nanoparticles for 1, 4, and 24 hours. Following the treatment, the cells were washed with DPBS and fixed using 4% paraformaldehyde in DPBS. The fluorescence images were obtained using the following filters: 585/29 and 624/40 for emission and excitation, respectively (Evos® FL, Thermo Fisher Scientific, Loughborough, Leicestershire, UK).

#### 3.2.2.5 Clathrin-mediated endocytosis inhibition using chlorpromazine

To inhibit clathrin-mediated endocytosis, SH-SY5Y cells were treated with chlorpromazine (5 μg/mL in DPBS) for 90 minutes. Before treatment with nanoparticles, the chlorpromazine-containing culture medium was removed, and the cells were washed twice using DPBS (101).

#### 3.2.2.6 Data processing and statistical analysis

Data calculation, graphs processing and statistical analysis were carried out using GraphPad Prism Software (California, USA). For paired data, statistical analysis was carried out using Student's t-test. Meanwhile, for groups of data, one-way ANOVA and post-hoc Dunnett's test for multiple comparisons were used. Flow cytometry data were processed using FlowJo Software (Ashland, OR, USA).

## 3.3 Results and discussion

### 3.3.1 Cytotoxicity of stabilisers

Assessing the compatibility with neuronal cells is an important part in developing nanoparticle-based carrier systems for nose-to-brain delivery. In this study, LNCs and PLGA-NPs nanoparticles that have been prepared and characterised were tested on SH-SY5Y neuroblastoma cells. As a first step, the toxicity of the stabiliser was studied to confirm that the free surfactant left in preparation would not affect the toxicity results.

Surfactants and polymeric stabilisers are commonly employed in nanoparticle preparations for various purposes, e.g. size control and surface modification (103). However, some surfactants and stabilisers may possess toxicity of their own (42, 43). In total, three different surfactants were tested: Kolliphor® HS15, poloxamer 407 and Kolliphor® P188. As shown in

Figure 12, the toxicity of the three surfactants used is concentration-dependent. For Kolliphor® HS15, the IC50 was calculated to be 0.225 ± 0.11 and 0.19 ± 0.1 mg/mL after 1 or 24-hour exposure, respectively (Table 5; Figure S2; Table S1). Statistical analysis showed no significant difference between the two time points, suggesting that the toxic effect of this surfactant occurs quickly. This concentration is at least ~127-times lower than the theoretical concentration of Kolliphor® HS15 in non-purified LNCs (~56.67 mg/mL for LNC50 and ~24.29 mg/mL for LNC100). This once again emphasizes the importance of purification process for LNC formulations.

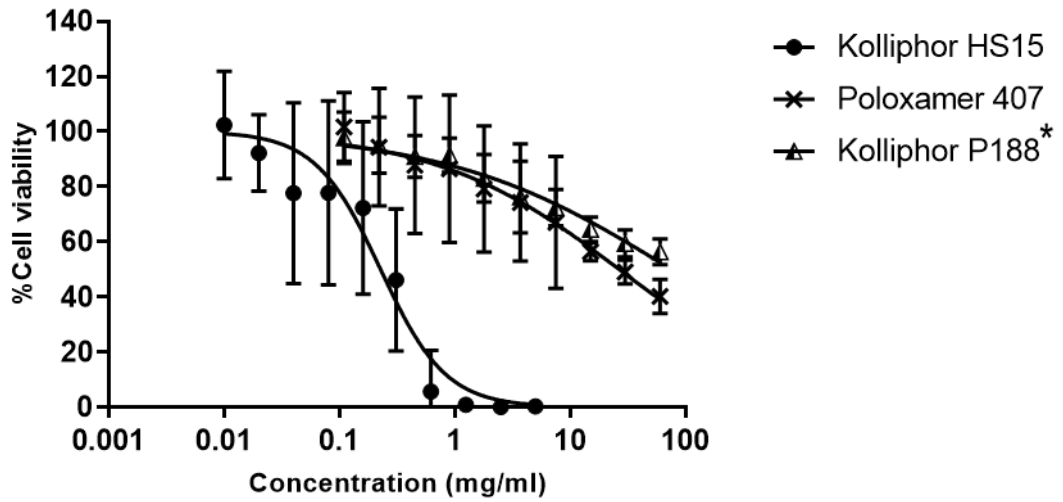


**Figure 12**. Cell viability of SH-SY5Y cells following 24-hour exposure of Kolliphor® HS15, poloxamer 407, and Kolliphor® P188. Data presented as mean ± SD from three independent experiments (*n*=3). Statistical analysis using paired t-test compared Kolliphor® P188 to poloxamer 407, *$p<0.05$. Comparison cannot be made with Kolliphor® HS15 because of the difference in concentration tested.

**Table 5**. IC50 of various surfactants towards SH-SY5Y cell following 24-hour exposure[(1)]

| Surfactant | IC50 | | CMC (M)[(4)] |
|---|---|---|---|
| | mg/mL[(2)] | M[(3)] | |
| Kolliphor® HS 15 | 0.19 ± 0.1 | $2.0 \times 10^{-4}$ | $1.3 \times 10^{-4}$ |
| Poloxamer 407 | 25.25 ± 2.3** | $2.0 \times 10^{-3}$ | $2.8 \times 10^{-6}$ |
| Kolliphor® P188 | 71.46 ± 9.3*** | $8.5 \times 10^{-3}$ | $4.8 \times 10^{-4}$ |

[(1)]Data presented as mean ± SD from three independent experiments ($n$=3)
[(2)]Statistical analysis using one-way ANOVA compared to IC50 of Kolliphor® HS15, $^{**}p<0.01$, $^{***}p<0.001$
[(3)]Calculated based on the average of IC50 shown on the table using average molecular weight: Kolliphor® HS15 = 960 g/mol, poloxamer 407 = 12,600 g/mol, Kolliphor® P188 = 8,400 g/mol
[(4)]Based on reference (53)

The poloxamer-based surfactants used in this study, poloxamer 407 and Kolliphor® P188, are generally considered to be safe and biocompatible (50). Thus, cytotoxicity assessment for the surfactant compound alone is not commonly studied. However, previous studies have revealed that amphiphilic poloxamers can interact with the lipid bilayer in cellular membranes, with or without disrupting its integrity (104, 105). Yet, it is still unclear whether this interaction is beneficial or not as poloxamers can act both as membrane sealant and permeabilizer (105). As membrane sealants, poloxamers have been shown to restore the membrane integrity of cells such as fibroblast and muscle cells (106, 107). On the other hand, as membrane permeabilizer, poloxamer may fluidify the membrane and increase uptake. For example, Salama *et al*. (108) reported an increase in brain drug concentrations following intranasal administration of nanocubic vesicles with poloxamers compared to unmodified, conventional liposomes. It was suggested that the enhanced brain accumulation was due to the ability of poloxamers to perturb the mucosal membrane in the nasal cavity. However, these studies used poloxamer concentrations below the critical micelle concentration (CMC) where no toxicity towards cells was observed.

The results of the toxicological evaluation of poloxamer 407 and Kolliphor® P188, revealed a significantly lower toxicity towards SH-SY5Y cells compared to Kolliphor® HS15 with IC50s of 25.25 ± 2.3 mg/mL and 71.46 ± 9.3 mg/mL after 24-hour exposure, respectively. Shorter exposure time was not tested for these poloxamer-based surfactants, considering that even after 24-hour, the toxicity at the highest concentrations tested resulted in only ~50% reduction of cell viability. It was also confirmed that the IC50s are much higher than the CMCs (Table 1), 710-fold for poloxamer 407 and 18-fold for Kolliphor® P188 and that poloxamer 407 is ~2.8x more toxic than Kolliphor® P188. In a study conducted by Frey, *et al*. (109), it was found that the interaction between poloxamers and the lipid bilayer is governed by the length of the hydrophobic PPO block where longer PPO blocks will have stronger interactions with membrane lipids. This result agreed with the findings from Chieng *et al*. (104) which showed that more hydrophobic polymers caused more disruption to lipid bilayer. As mentioned in the previous chapter, poloxamer 407 is more hydrophobic than Kolliphor® P188 with 2.2x longer PPO chain. It was also interesting to note that, for poloxamer-based surfactants, toxicity only occurs at concentrations much higher than the CMC where rapid solubilisation of lipid bilayer takes place (104).

For Kolliphor® HS15, Maupas, *et al*. (2011) found that the IC50 of Kolliphor® HS15 towards HaCaT cells ($17.0 \pm 0.8 \times 10^{-5}$ mg/mL or ~$1.73 \times 10^{-7}$ M) was lower than its CMC (43). In this study, the IC50 of Kolliphor® HS15 is marginally (ca. 1.5-fold) higher than its CMC. This indicates that the toxicity caused by Kolliphor® HS15 is not solely a consequence its ability, as a surfactant, to solubilise cell membranes. Another hypothesis proposed regarding the mechanism of the toxicity is related to the presence of fatty acid stearates in the surfactant that had been proven to induce apoptosis through induction of NFκ-B and IKK activation (42, 110).

### 3.3.2 Cytotoxicity of LNCs

The viability of SH-SY5Y cells following exposure to purified LNCs at different time points is presented in Figure 13. The results showed that both LNC50 and LNC100 exhibited concentration-dependent toxicity. No differences in toxicity were observed between the two LNC sizes when cells were treated for 1 or 4 hours, with IC50 values of ca. 3.5-5 mg/mL in both cases (Table 6). Longer exposure times led to decreases in IC50 for both nanoparticle formulations with LNC50 experiencing a more drastic change. Indeed, the IC50 for LNC50 decreased ~8.6-fold between 1 and 72 hours, while the change was only ~3.7-fold for LNC100 within the same time frame. The results showed that smaller LNCs are slightly more toxic than larger ones. The effect of particle size on nanoparticle toxicity has been studied throughout the years and most of the findings show higher toxicity come from nanoparticle with smaller size (30). This phenomenon is in a good agreement with a recent study conducted by Le Roux, *et al*. (42) which concluded that smaller LNCs are more toxic. However, that study did not involve a purification step, thus the toxic effect was likely linked to the high concentration of surfactant needed for smaller size LNCs.

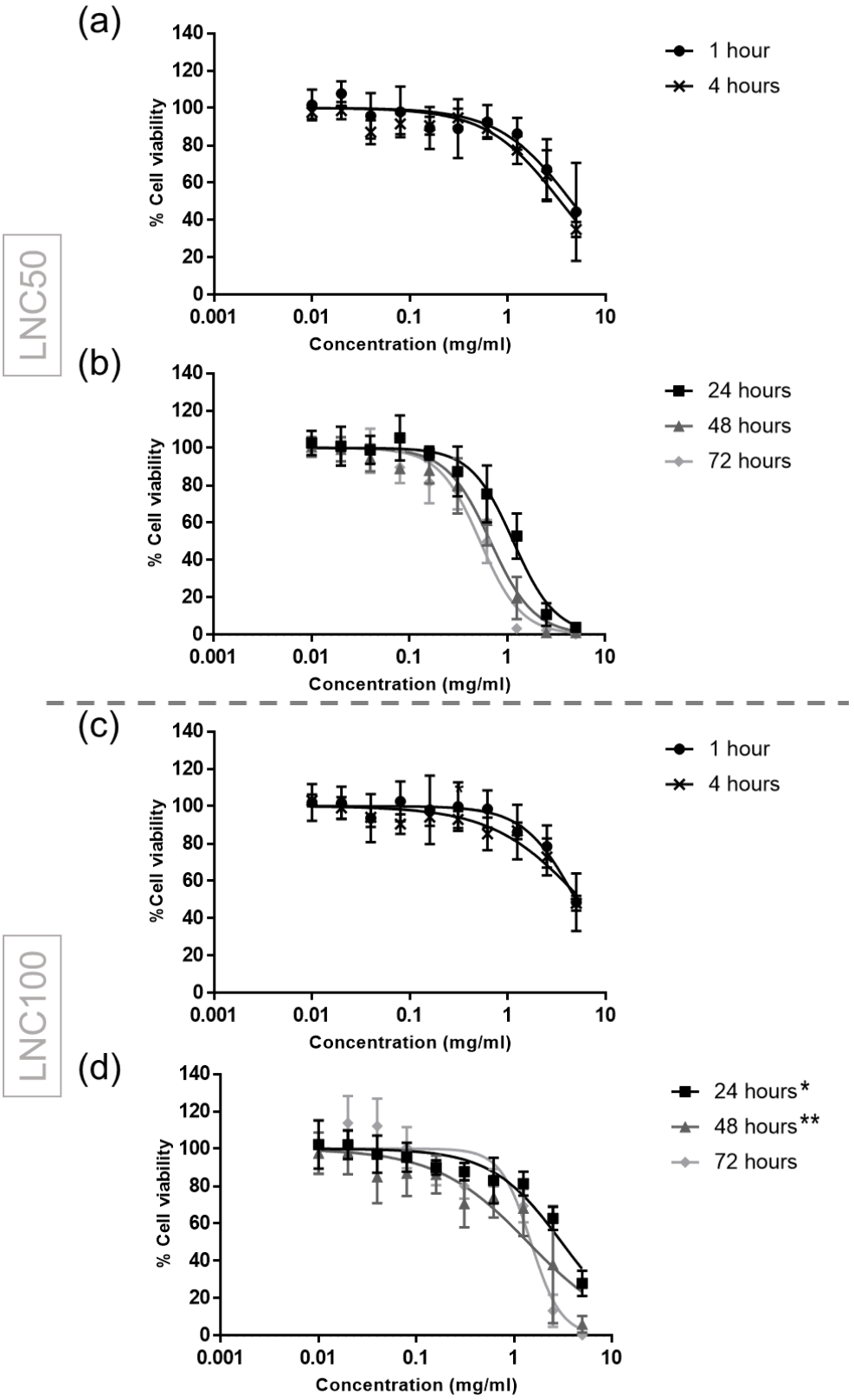


**Figure 13.** Cell viability of SH-SY5Y following exposure of LNC50 (a,b) and LNC100 (c,d) at different time points. Data are presented as mean ± SD from three independent experiments (*n*=3). Statistical analysis using one-way ANOVA compared to the lowest treatment duration (1 hour) for each LNC, **p<0.05, **p<0.01*.

**Table 6.** IC50 of LNCs to SH-SY5Y cells following treatment within different exposure time[(1)]

| Exposure time (hours) | IC50 (mg/mL) | |
|---|---|---|
| | LNC50[(2)] | LNC100[(3)] |
| 1 | 4.54 ± 2.3 | 5.36 ± 1.9 |
| 4 | 3.46 ± 0.4 | 5.32 ± 0.8 |
| 24 | 1.16 ± 0.1$^{*}$ | 3.05 ± 0.3 |
| 48 | 0.67 ± 0.1$^{*}$ | 1.69 ± 1.4$^{*\alpha}$ |
| 72 | 0.53 ± 0.1$^{*}$ | 1.43 ± 0.2$^{*\alpha}$ |

[(1)]Data presented as mean ± SD from at least three independent experiments
[(2)]Statistical analysis using one-way ANOVA compared to IC50 of 1-hour exposure for each LNC, $^{*}p<0.05$
[(3)]Statistical analysis using *t-test* compared with LNC50 at the same exposure time, $^{\alpha}p<0.05$

The manufacture method for LNCs in this study involved a purification process; as a consequence, one cannot simply link the cytotoxicity to the surfactant alone. Prior to testing on cell culture, purification had successfully reduced surfactant concentration to <LoQ. Although this concentration is still higher than the IC50 of Kolliphor® HS15, particles were diluted at least 11- or 14-fold to produce the highest concentrations tested. Thus, it would be expected that, even at the highest LNC concentration, the concentration of free surfactant would be well below its IC50. Despite this, the effect of the surfactant on the toxicity cannot be completely abolished. Indeed, the release of the remaining surfactant molecules during incubation in the cell culture is still expected (111). This might actually explain the slightly more toxic effect of LNC50 compared to LNC100. Theoretically, at the same dose given in mg/mL, LNC50 have twice the surface area of LNC100 (1142 $cm^2$ and 571 $cm^2$ at concentration 1 mg/mL, respectively). A larger specific surface area will allow more interaction between nanocapsule surface and the surrounding environment, including the cells. Here, it was possible to calculate

that the particle number dose is 8-fold higher for LNC50, compared to LNC100 at the same concentration-dose (mg/mL). Interestingly, when comparing the toxicity at the same particle/cell ratio, LNC100 showed higher toxicity.

In an attempt to assess the ability of cells to recover from LNC exposure, cells were left to recover for 24, 48, and 72 hours after treatment (Figure 14). The results showed that for LNC50, recovery was delayed after exposure to concentrations above, but not below, the IC50 IC50 (1.16 ± 0.1 mg/mL). Encouragingly, recovery was significant after treatment with 0.32 mg/mL LNC50. On the other hand, for LNC100, recovery was impaired even at concentrations below the IC50 (1.25 and 2.5 mg/mL). Two mechanisms may be involved in the continuous cell death after recovery phase caused by both LNCs. The first mechanism can be linked to the activation of intrinsic mechanism of cell death caused by the LNCs that have entered the cells. The second mechanism is related to the cell itself. The SH-SY5Y cell line requires sufficient cell-to-cell communication for cell growth. Exposure to high LNCs concentrations may have caused the cell number to become sparse, leading to more cell death in the culture (90). This will need to be investigated further, but may influence the dosing frequency, especially if nanoparticles are in close contact will cell membranes, which will likely be the case for nose-to-brain administration.

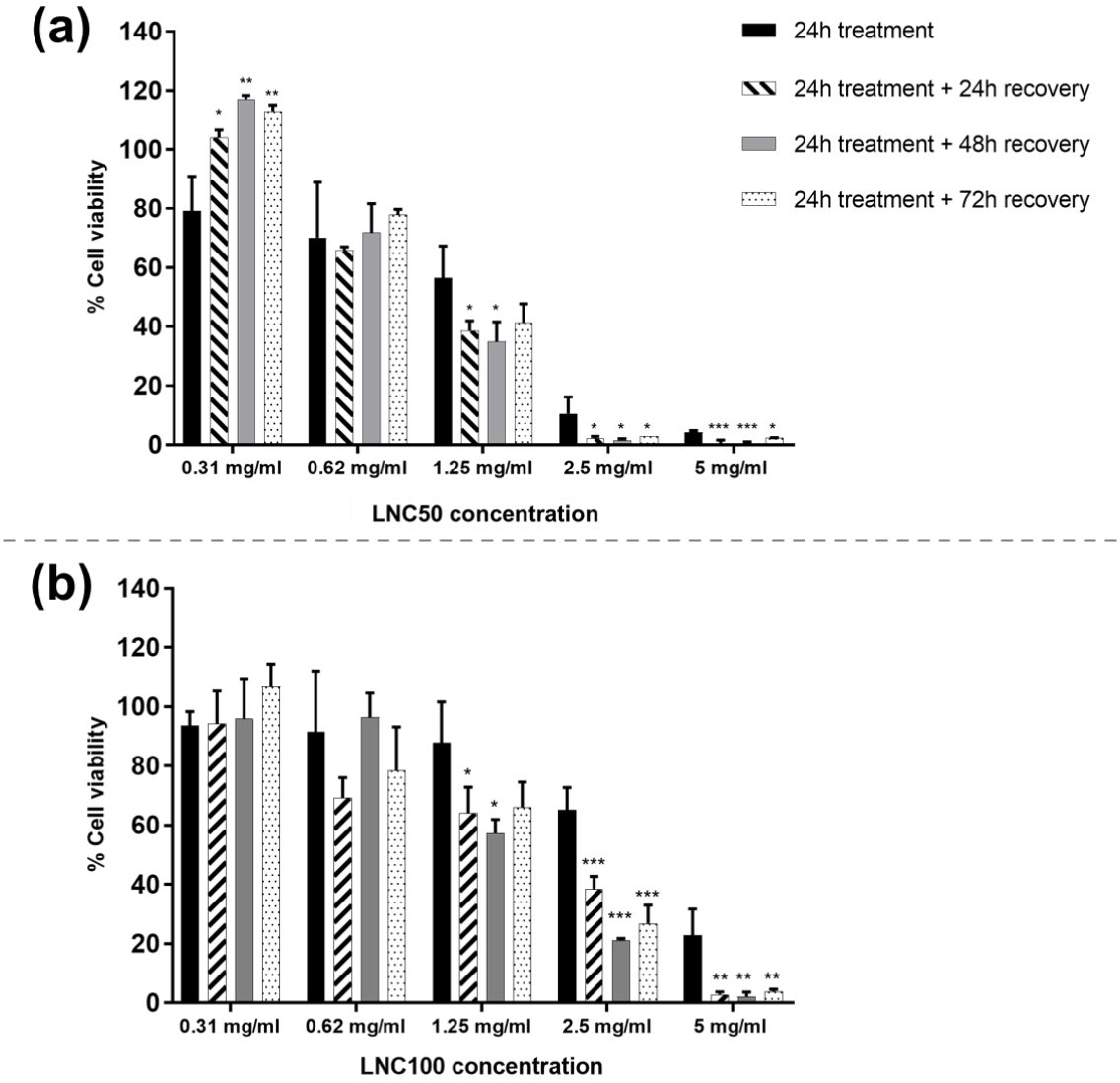


**Figure 14**. Cell viability of SH-SY5Y after recovery phase following 24-hour LNC exposure, (a) LNC50 and (b) LNC100. Data presented as mean ± SD from three independent experiments (*n*=3). Statistical analysis using one-way ANOVA compared to the 24-hour treatment at the same given concentration, **p<0.05, **p<0.01 and ***p<0.001*.

### 3.3.3 Cytotoxicity of PLGA-NPs

Figure 15 presents the cell viability of SH-SY5Y cells following exposure to PLGA-NPs. The toxicity profiles of PLGA-NPs prepared with two different stabilisers, poloxamer 407 and Kolliphor® P188), were similar. The characterisation for both formulations showed similar properties in terms of particle size and surface charge which may have contributed to this finding. The particle size for the PLGA-NPs obtained was 179.2 ± 4.2 nm and 162.1 ± 1.0 nm for PLGA-P407 and PLGA-K188, respectively. There was no significant difference in the IC50 (Table 7) between different exposure times and between different stabilisers at the same exposure time.

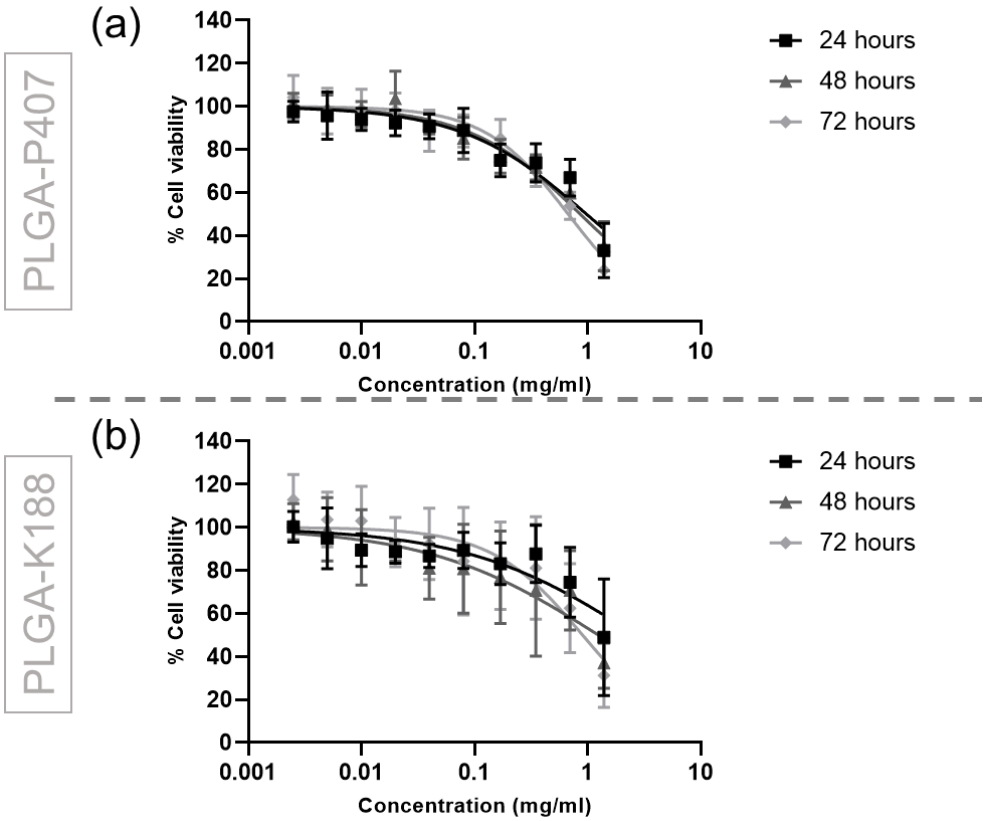


**Figure 15**. Cell viability of SH-SY5Y cells following exposure with (a) PLGA-P407 and (b) PLGA-K188 after 24, 48 and 72 hours. Data presented as mean ± SD from three independent experiments (*n*=3). Statistical analysis using one-way ANOVA found no significant difference compared to the lowest treatment duration (24 hours) for each PLGA-NP.

**Table 7**. IC50 of PLGA-NPs to SH-SY5Y cells following treatment within different exposure time[(1)]

| Exposure time (hours) | IC50 (mg/mL) | |
|---|---|---|
| | **PLGA-P407** | **PLGA-K188[(2)]** |
| 24 | 1.013 ± 0.37 | 1.148 ± 0.68 |
| 48 | 0.855 ± 0.06 | 1.010 ± 0.72 |
| 72 | 0.724 ± 0.54 | 0.858 ± 0.48 |

[(1)]Data presented as mean ± SD from three independent experiments ($n$=3)
[(2)]Statistical analysis using paired t-test found no significant difference between two different types surfactants used

PLGA is a biodegradable polymer and usually praised for its biocompatibility (80). Likewise, the stabilisers used to prepare the nanoparticles are also generally non-toxic. The use of poloxamer-based surfactants as stabiliser for PLGA-NPs has been suggested in a large number of studies because of their ability to provide steric stabilisation. Surprisingly, the IC50s obtained for the PLGA-NPs shown above are ~5x lower than those obtained both LNCs. Unlike LNCs, surfactant-related toxicity is not expected from PLGA-NPs. It is also hypothesised that the release of the surfactant molecules into media is more unlikely as the PLGA polymer itself is amorphous with relatively high glass transition temperature (~45 $^{o}$C), leading to a more rigid structure (81, 112).

Overall, the results showed that both LNCs and PLGA-NPs are compatible with SH-SY5Y as the toxicity only occurred at relatively high concentrations. This finding may be useful for the dose adjustment of the nanoparticles to be used within a safe range for nose-to-brain delivery. Additionally, as the nanoparticles may be absorbed directly into the systemic circulation, following intranasal application, the dilution experienced should be enough to bring the particles concentration far below the IC50. Thus, minimum systemic toxicity is expected.

### 3.3.4 Cellular uptake of nanoparticles

Another important aspect of cell-nanoparticle interactions to be assessed is cellular uptake. For that purpose, nile red, a lipophilic fluorescent dye, was incorporated in LNCs and PLGA-NPs. Flow cytometric analysis has shown that both LNC50 and LNC100 were taken up by SH-SY5Y cells in a concentration-dependent pattern (Figure 16a and 16b). Meanwhile, quantification of median fluorescence intensity (MFI) from the flow cytometric data (Figure 16c) showed interesting results. It was found that the fluorescence intensity was significantly higher following incubation with LNC100 compared to LNC50 at the same concentration. This result was also confirmed using fluorescence microscopy (Figure 17 and 18). This result contradicts the common perception that smaller nanoparticles have higher uptake rate (23). Indeed, Paillard *et al*. (2010) had demonstrated lower uptake of 100 nm LNCs compared to smaller sizes in glioma cells (113). However, although this result could simply be interpreted as proof that the uptake of LNC100 is higher than that of LNC50, there are several factors that may lead to higher fluorescence intensity for the larger particles and less information is available on the interaction of LNC100 with cells due to most studies focusing on LNC50. One of the drawbacks in using flow cytometry to analyse fluorescent-labelled nanoparticle uptake is that it cannot provide the location of the nanoparticles whether they are internalised or simply associated with cellular membrane (114). Nevertheless, as the experiment involved rinsing prior to analysis, this indicates that the interaction of membrane-attached nanoparticles is rather strong. Besides that, leakage and transfer of dye could also occur during incubation, thus, the overall data may not reflect the actual uptake of nanoparticles. In a recent study conducted by Simonsson, *et al*. (115), rapid transfer of the dye was detected from nile read-loaded LNCs to THP-1 (human monocyte/macrophage) cells and from nile read loaded-LNCs to unloaded-LNCs. It is suggested that the dye exchange can occur as long as the receptor (either cells or

unloaded-LNCs) possess lipid compartment (115). A similar phenomenon was observed by Bastiat *et al.*(116) in HEI-OC1 (auditory cells) and by Klymchenko *et al*. (117) in HeLa (cervical cancer) cells. However, the size of the LNC observed in the aforementioned studies was 60 nm, while this is may be the case as well for LNC50, a more extensive dye transfer seems to have occurred with LNC100. This may indicate more extensive dye leaching with LNC100 in the media or simply that the particles or dye accumulated in cells through a passive mechanism.

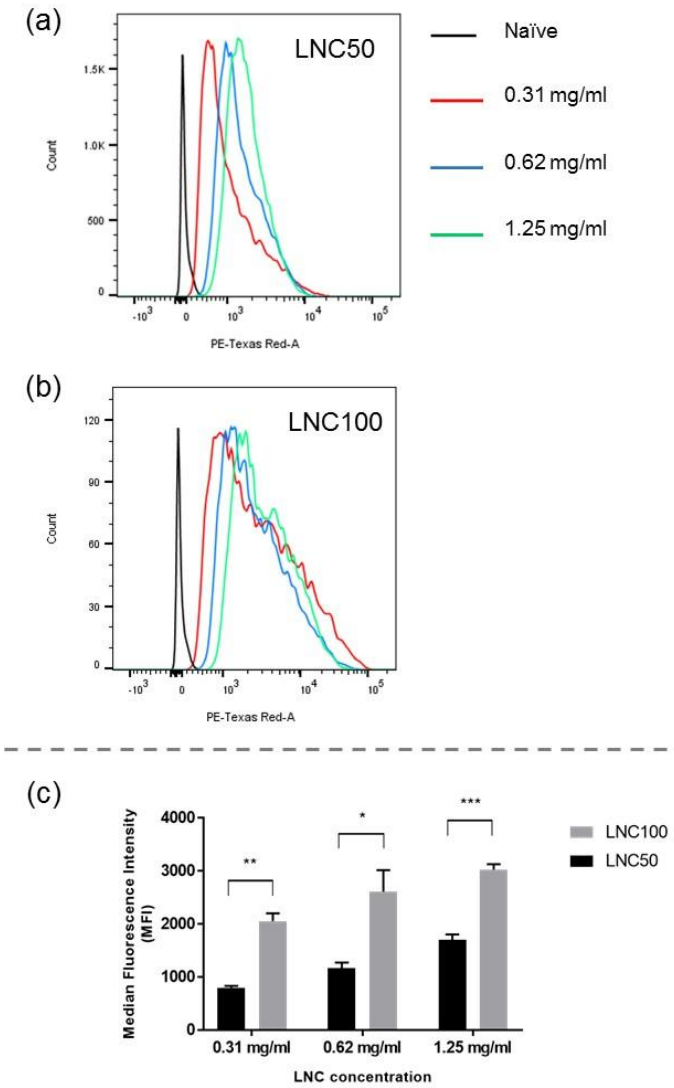


***Figure 16.*** *(a, b) Flow cytometry histogram of fluorescent intensity in SH-SY5Y cells following 24-hour treatment with LNCs, (c) Median fluorescence intensity of nile red in SH-SY5Y cells following 24-hour treatment with LNCs, presented as mean ± SD of three* independent experiments (*n*=3). Statistical analysis using paired t-test, compared between two LNCs at the same given concentration, *p<0.05, **p<0.01, ***p<0.001.

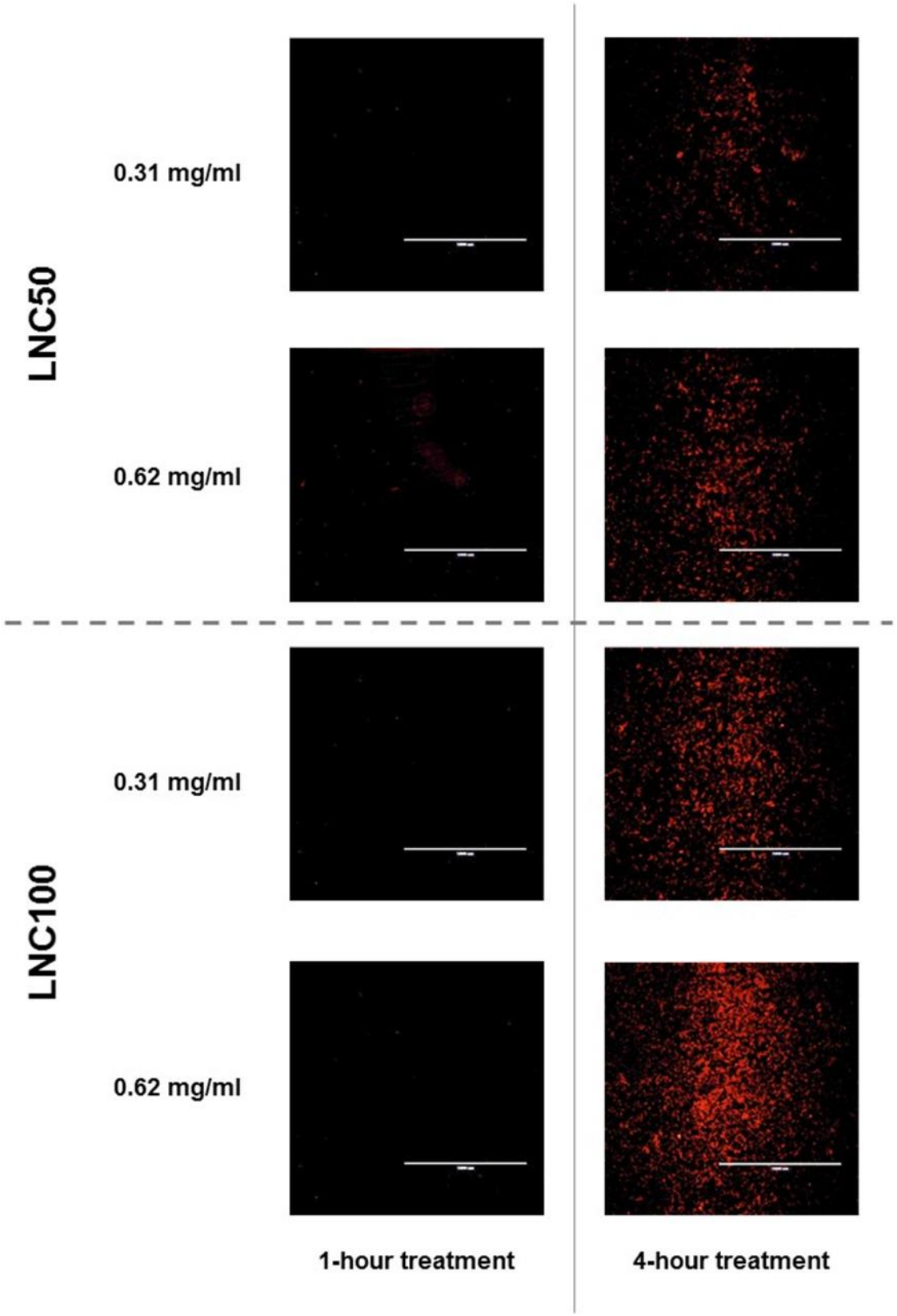


**Figure 17**. Fluorescence microscopy imaging of SH-SY5Y cells following 1- and 4-hour exposure with nile-red loaded LNCs (Total magnification = 40x, scale bar = 1000 μm).

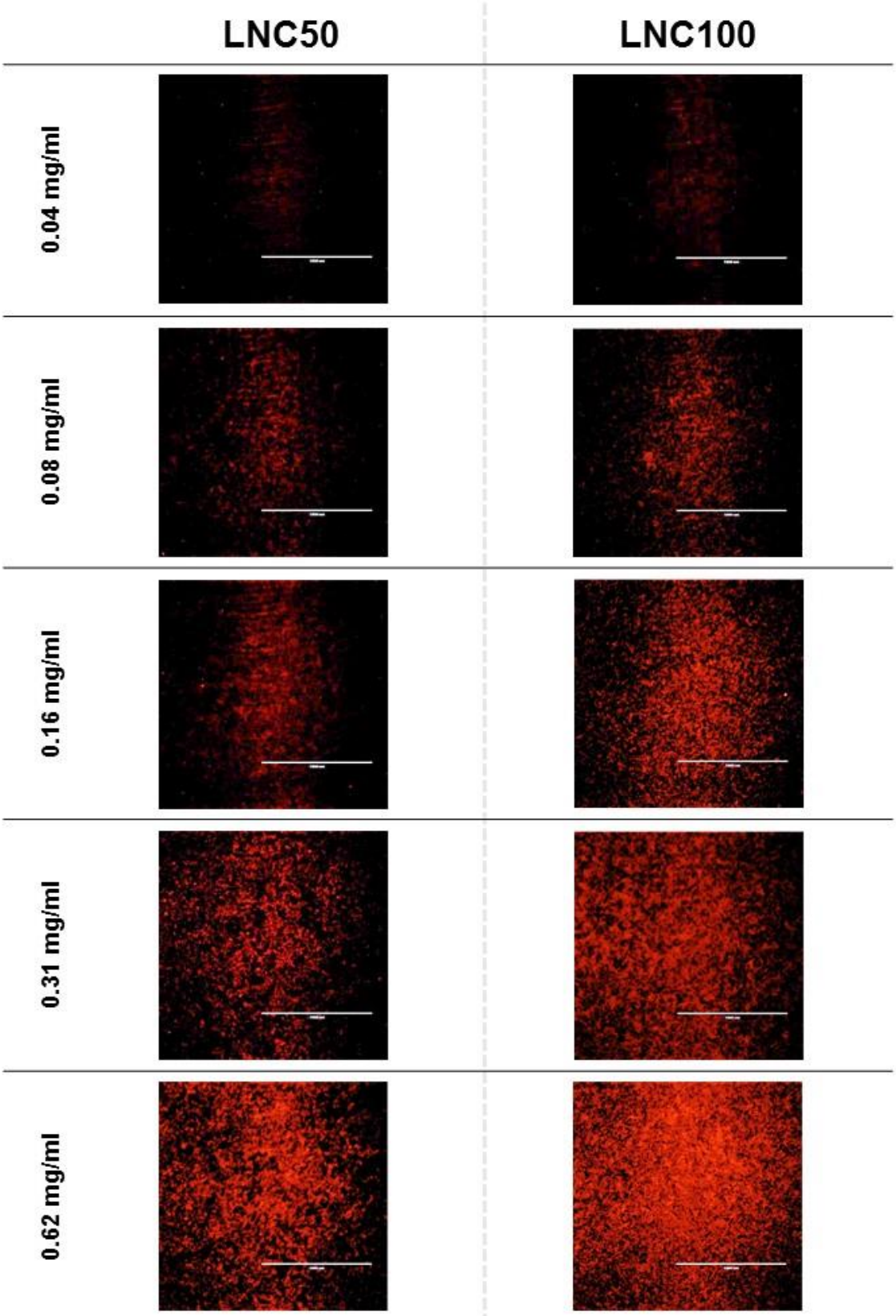


**Figure 18.** Fluorescence microscopy imaging of SH-SY5Y cells following 24-hour exposure of nile red loaded LNCs at different concentrations (Total magnification = 40x, scale bar = 1000 μm).

The kinetic study of cellular uptake for LNCs, also analysed using flow cytometry, demonstrated higher nile red internalisation into the cells for LNC100 compared to LNC50 (Figure 19). From the flow cytometry data, the percentage of fluorescent cells was obtained by comparing the treatment to the control. After 2 hours of incubation with LNC concentration of 0.31 mg/mL, the percentage of fluorescence cells was almost 100% for LNC100, whereas LNC50 only ~40%.

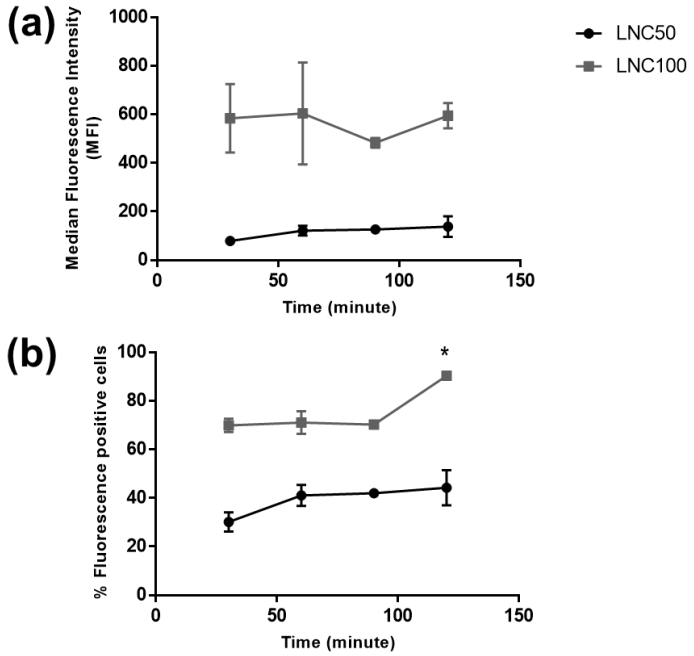


**Figure 19**. Cellular uptake kinetic of nile read-loaded LNCs in SH-SY5Y cells presented as (a) median fluorescence intensity (MFI) and (b) % fluorescence positive cells. Data presented as mean ± SD from three independent experiments ($n$=3). Statistical analysis using one-way ANOVA compared to the initial measurement at the same treatment condition, $*p<0.05$.

Previous studies have confirmed that clathrin-mediated endocytosis (CME) plays a major role in nanoparticle uptake by neurons (118, 119). This endocytic mechanism allows the uptake of nanoparticles with size between 50 - 200 nm (120) and can be inhibited by chlorpromazine (CPZ). Here, CPZ-inhibition seemed to have lowered the fluorescence intensity following treatment with LNC50, but not LNC100 (Figure 20). The fluorescence signal detected for

LNC50 seems to result from a combination of actual particle endocytosis (ca. 35 - 50%) and membrane adsorption/passive diffusion/dye exchange.

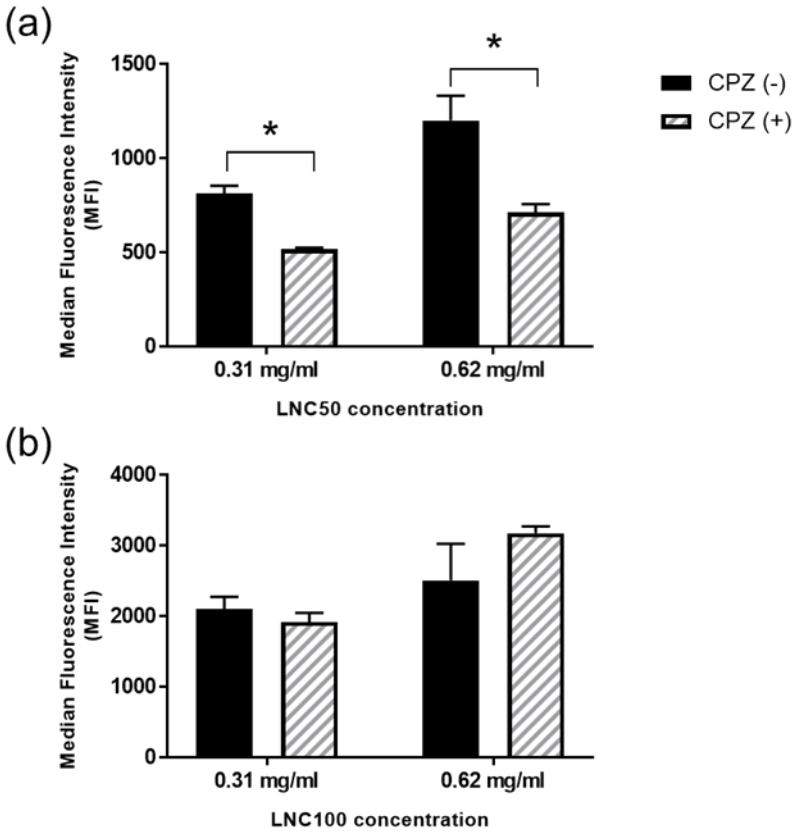


**Figure 20**. Cellular uptake (24-hour treatment) of nile red-loaded (a) LNC50 and (b) LNC100 into SH-SY5Y compared to chlorpromazine perturbed [CPZ (+)]. Data presented as mean ± SD of three independent experiments ($n$=3). Statistical analysis using t-test between the same treatment concentration, $*p<0.05$.

For PLGA-NPs, nanoparticle uptake through active endocytic mechanism in SH-SY5Y cells has been demonstrated in recent studies (91, 121). However, in this study, in contrast to LNCs, PLGA-NPs did not seem to be uptaken by cells to the same extent (Figure 21). PLGA-P407 was not taken up by the SH-SY5Y cells, whereas a small number of PLGA-K188 were internalised, but only at higher concentrations. This could simply be explained by the significantly lower fluorescence signal of the dye incorporated in PLGA-NPs compared to LNCs at the same given concentration in mg/mL (~10x lower). Consequently, this indicates the limitation of the method used where the analysis depends on the loading of the fluorescence

dye. Finding a suitable dye for this type of nanoparticle may be an alternative option in the future that can provide more accurate information regarding cellular uptake.

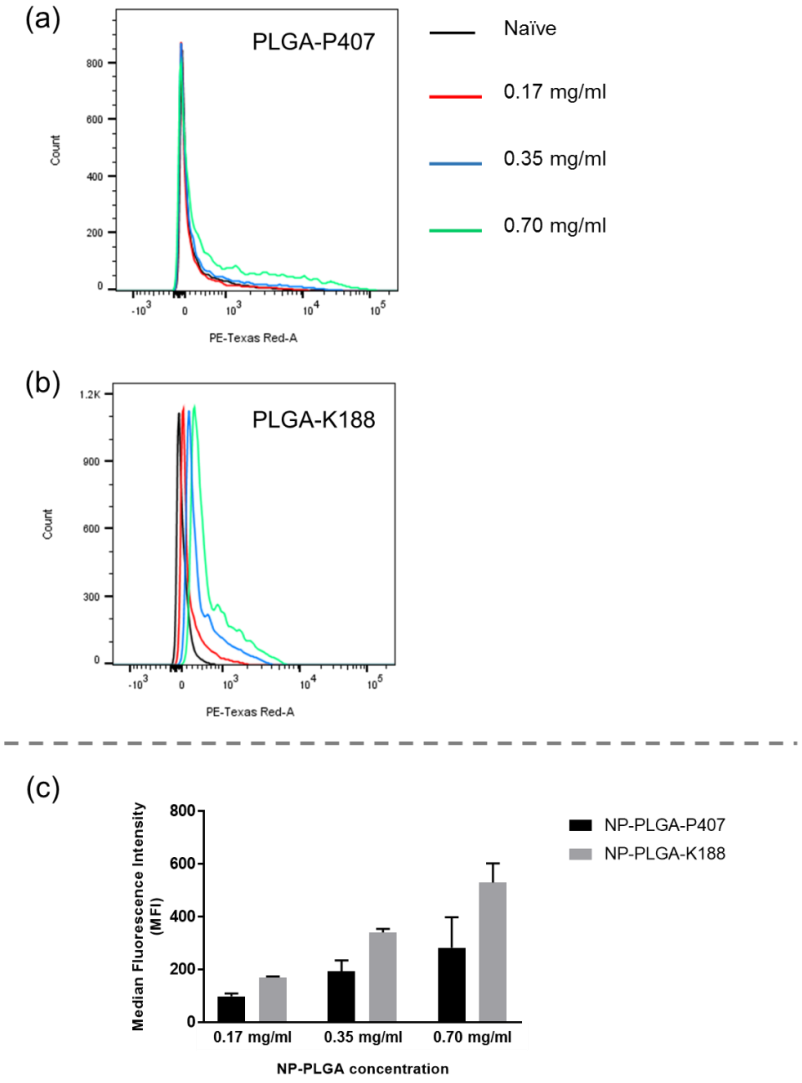


**Figure 21**. (a, b) Flow cytometry histogram of fluorescent intensity in SH-SY5Y cells following 24-hour treatment with PLGA-NPs, (c) Median fluorescence intensity of nile red in SH-SY5Y cells following 24-hour treatment with PLGA-NPs, presented as mean ± SD of three independent experiments (*n*=3). No significant difference was found between the uptake of two types of PLGA NPs.

## 3.4 Conclusion

The cytotoxicity assessment of LNCs and PLGA-NPs prepared in this study showed a time- and concentration-dependent pattern. Interestingly, the toxicity profile of LNC formulations differs on whether the dose is compared as mg/mL or particle/cell ratio. LNC100 showed higher cellular uptake, however, this is may be due to dye exchange without the nanoparticles being necessarily uptaken. PLGA-NPs were generally found to be more toxic compared to LNCs and there was no significant difference between the different stabilisers used. Further assessment is required to understand the mechanisms leading to cell death, i.e. measurement of apoptosis or reactive oxygen species (ROS) production.

# 4. Conclusion and future outlook

## 4.1 Conclusion

Following the manufacturing step of LNCs and PLGA- NPs, the nanoparticle formulations were characterised for their physicochemical properties, including particle size, surface charge, and surface hydrophobicity.

For the LNCs, it is possible to control the intended size of the nanocapsules by varying the ingredients' proportions. Three different sizes of LNCs were prepared, LNC20, LNC50, and LNC10. Because of the high concentration of surfactant used during preparation, purification by dialysis was conducted. However, it was found that this dialysis method was not sufficient to purify the LNC20 formulations. Thus, LNC20 was removed from further studies, due to the risk of toxicity from the high concentrations of free surfactant. For the PLGA-NPs, the nanoparticles were prepared using two different poloxamer-based surfactants to understand the impact of using different stabilisers, namely poloxamer 407 and Kolliphor® P188. There was no significant difference in terms of particle size, PdI, and surface charge for both LNC50 and LNC100 before and after purification and no significant difference was found for the PLGA-NPs between the two stabilisers.

Surface hydrophobicity for the nanoparticles was also studied using two test methods: 1) salt aggregation test and 2) hydrophobic interaction chromatography. The results obtained from the SAT were comparable between the nanoparticles. From this test, it was found that LNC50 has a slightly more hydrophobic surface compared to LNC100 and that PLGA-NPs, PLGA-K188 were slightly more hydrophobic compared to PLGA-P407. For both particle types, it was hypothesised that any difference observed was due to the arrangement of surfactant/stabiliser on the nanoparticle's surface which could leave hydrophobic regions exposed. The results from HIC analysis agreed with the SAT test, showing the HIC index of both LNCs <0.7, suggesting

a more hydrophilic surface, compared to both PLGA-NPs with HIC index >0.7. Both methods have their own advantages and disadvantages. The SAT method can easily be applied to different particles and the test can be performed at physiological temperature. Meanwhile, HIC was able to detect small differences between particles, even at room temperature. Further studies will be required to determine which one of the two methods best predict *in vivo* behaviour for a wide range of nanoparticles and routes of administration.

After that, the nanoparticle formulations were assessed for their compatibility and interaction with SH-SY5Y cells, as a neuronal cell model. Because of the emerging importance of toxicological studies of nanomaterials, cytotoxicity assessment based on mitochondrial activity was carried out. The assessment was conducted not only on the nanoparticle formulations but also on the stabilisers alone. The results showed that Kolliphor® HS15 (used for LNCs) is significantly more toxic than poloxamer 407 and Kolliphor® P188 (used for PLGA-NPs). This emphasizes the importance of purification step for LNCs formulation and for any nanoparticle made from similar surfactant. Meanwhile, poloxamer 407 was found to be ~2.8x more toxic that Kolliphor® P188, probably due to a stronger interaction of the more hydrophobic poloxamer 407 with the lipid bilayer, which may result in more disruption of the cell membrane compared to Kolliphor® P188.

The cytotoxicity assessment of LNCs towards SH-SY5Y cells showed a concentration- and time-dependent pattern. The cell studies for LNC formulations were only carried out on the purified LNCs. At the same concentration (mg/mL) LNC50 were found to be more toxic than larger particles; however, if comparing equivalent particle/cell ratio dose, than LNC100 were more toxic. This confirms that care should be taken when comparing the toxicity of particles with the same composition, but not the same size. For the PLGA-NPs, there was no significant difference of toxicity profile between two formulations, independently of the stabiliser used.

Cellular uptake was also studied using flow cytometry and fluorescence microscopy. Nile red, a lipophilic fluorescent dye, was incorporated into nanoparticles for this assessment. However, it is impossible to compare between LNCs and PLGA-NPs as there is a significant difference in terms of fluorescent signal. For the LNCs, the results showed higher fluorescence intensity following treatment with LNC100 compared to LNC50. Although it could be simply interpreted as a higher uptake, it may not be the case in this study. Inhibition of clathrin-mediated endocytosis decreased the uptake of LNC50, but not LNC100, indicating that something other than active uptake is involved. One possibility is that dye exchange has occurred and may have been more extensive for LNC100, for reasons that will need to be determined. For the PLGA-NPs, cellular uptake was observed to occur to a very small extent, though it is not clear whether this was due to low loading of the dye, low uptake of the larger particles by the cells or a combination of both.

To conclude, this study assessed the interaction between two type of organic nanoparticles, LNCs and PLGA-NPs, with neuronal cell mode as candidates of nanocarrier system for nose-to-brain delivery. The cytotoxicity assessment showed that the toxic effect of the nanoparticles towards the cells is influenced by the physicochemical characteristics of the nanoparticles produced. However, both LNCs and PLGA-NPs can be categorised as biocompatible for the SH-SY5Y cells. The cellular uptake studies showed interesting results for LNC formulations where the larger LNC100 showed higher extent of dye uptake, which contradicts the long-believed theory that smaller nanoparticles are ingested more by the cells. However, dye transfer may be the reason behind this phenomenon. In terms of their role as drug carrier system, LNCs have been found to be suitable with some anticancer and antimicrobial drugs. This will enable the researchers in this field to develop LNC-drug formulations for CNS-related cancer or

infection (111, 122). However, this does not limit the application of this particular system for other type of drugs, e.g. antipsychotic agents or treatment for neurodegenerative disorders.

## 4.2 Future work

This study has provided preliminary answers regarding the interaction between nanoparticles and neuronal cell, though this was based on the use of SH-SY5Y neuroblastoma cell line, as neuronal cell model. However, several questions have also arisen that will require further assessment in order to identify the most suitable nanocarrier system for nose-to-brain delivery. The suggestion for future works, include, but are not limited to the following:

1. In-depth assessment of cellular death mechanism following purified LNCs (with low remaining surfactant concentration).
2. Finding of a more effective purification method to enable preparation of smaller LNCs with maximum removal of surfactant following preparation.
3. Finding a more suitable fluorescent dye for cellular uptake study for LNCs and PLGA-NPs to allow a more accurate prediction of nanoparticle uptake.

Seeing as nose-to-brain delivery is a promising and emerging field of research, further studies regarding the specific mechanism of nanoparticulate uptake and transport are imperatively required. For this purpose, *in vitro* testing using other cell models involved in intranasal absorption, e. g. nasal mucosae and olfactory ensheathing cells (OEC), will be useful models to use in the next steps of this project, along with primary neurons. Additionally, only two nanoparticles types were evaluated here; additional studies regarding other types of nanoparticle, either with different morphology (non-spherical) or different chemical composition (inorganic, protein, other lipids or polymer) may provide broader understanding of the impact of shape and composition. This will enable us to obtain

sufficient information in selecting and developing the most suitable nanocarrier system for nose-to-brain delivery.

# 5. References


1. WHO. Neurological Disorders: public health challenges. Switzerland: World Health Organization; 2006.

2. WHO. The top 10 causes of death (Fact Sheet No. 310): World Health Organization; 2015 [updated January 2017. Available from: http://www.who.int/mediacentre/factsheets/fs310/en/.

3. Craparo EF, Bondi ML, Pitarresi G, Cavallaro G. Nanoparticulate systems for drug delivery and targeting to the central nervous system. CNS neuroscience & therapeutics. 2011;17(6):670-7.

4. Koo Y-EL, Reddy GR, Bhojani M, Schneider R, Philbert MA, Rehemtulla A, et al. Brain cancer diagnosis and therapy with nanoplatforms. Advanced Drug Delivery Reviews. 2006;58(14):1556-77.

5. Pardridge WM. The Blood-Brain Barrier: Bottleneck in Brain Drug Development. NeuroRx: The Journal of the American Society for Experimental NeuroTherapeutics. 2005;2(1):3-14.

6. Azad TD, Pan J, Connolly ID, Remington A, Wilson CM, Grant GA. Therapeutic strategies to improve drug delivery across the blood-brain barrier. Neurosurgical focus. 2015;38(3):1-10.

7. Claudio P, Reatul K, Brigitte E, Geraldine P. Drug-delivery nanocarriers to cross the blood–brain barrier. In: Grumezescu AM, editor. Nanobiomaterials in Drug Delivery: William Andrew Publishing; 2016. p. 333-70.

8. Demeule M, Régina A, Jodoin J, Laplante A, Dagenais C, Berthelet F, et al. Drug transport to the brain: key roles for the efflux pump P-glycoprotein in the blood–brain barrier. Vascular Pharmacology. 2002;38(6):339-48.

9. Illum L. Is nose-to-brain transport of drugs in man a reality? The Journal of pharmacy and pharmacology. 2004;56(1):3-17.

10. Mistry A, Stolnik S, Illum L. Nanoparticles for direct nose-to-brain delivery of drugs. International journal of pharmaceutics. 2009;379(1):146-57.

11. Dasgupta A, Liu M, Ojha T, Storm G, Kiessling F, Lammers T. Ultrasound-mediated Drug Delivery to the Brain: Principles, Progress and Prospects. Drug discovery today Technologies. 2016;20:41-8.

12. Rapoport SI. Osmotic Opening of the Blood–Brain Barrier: Principles, Mechanism, and Therapeutic Applications. Cellular and Molecular Neurobiology. 2000;20(2):217-30.

13. Djupesland PG, Messina JC, Mahmoud RA. The nasal approach to delivering treatment for brain diseases: an anatomic, physiologic, and delivery technology overview. Therapeutic Delivery. 2014;5(6):709-33.

14. Agrawal M, Saraf S, Saraf S, Antimisiaris SG, Chougule MB, Shoyele SA, et al. Nose-to-brain drug delivery: An update on clinical challenges and progress towards approval of anti-Alzheimer drugs. Journal of Controlled Release. 2018;281:139-77.

15. Chow HS, Chen Z, Matsuura GT. Direct transport of cocaine from the nasal cavity to the brain following intranasal cocaine administration in rats. Journal of Pharmaceutical Sciences. 1999;88(8):754-8.

16. Westin UE, Bostrom E, Grasjo J, Hammarlund-Udenaes M, Bjork E. Direct nose-to-brain transfer of morphine after nasal administration to rats. Pharmaceutical Research. 2006;23(3):565-72.

17. Hada N, Netzer WJ, Belhassan F, Wennogle LP, Gizurarson S. Nose-to-brain transport of imatinib mesylate: A pharmacokinetic evaluation. European Journal of Pharmaceutical Sciences. 2017;102:46-54.

18. Mittal D, Ali A, Md S, Baboota S, Sahni JK, Ali J. Insights into direct nose to brain delivery: current status and future perspective. Drug Delivery. 2014;21(2):75-86.

19. Guastella AJ, Einfeld SL, Gray KM, Rinehart NJ, Tonge BJ, Lambert TJ, et al. Intranasal Oxytocin Improves Emotion Recognition for Youth with Autism Spectrum Disorders. Biological Psychiatry. 2010;67(7):692-4.

20. Pedersen CA, Gibson CM, Rau SW, Salimi K, Smedley KL, Casey RL, et al. Intranasal oxytocin reduces psychotic symptoms and improves Theory of Mind and social perception in schizophrenia. Schizophrenia Research. 2011;132(1):50-3.

21. Born J, Lange T, Kern W, McGregor GP, Bickel U, Fehm HL. Sniffing neuropeptides: a transnasal approach to the human brain. Nature neuroscience. 2002;5(6):514-6.

22. Dhuria SV, Hanson LR, Frey WH. Intranasal delivery to the central nervous system: Mechanisms and experimental considerations. Journal of Pharmaceutical Sciences. 2009;99(4):1654-73.

23. Behzadi S, Serpooshan V, Tao W, Hamaly MA, Alkawareek MY, Dreaden EC, et al. Cellular uptake of nanoparticles: journey inside the cell. Chemical Society Reviews. 2017;46(14):4218-44.

24. Blanco E, Shen H, Ferrari M. Principles of nanoparticle design for overcoming biological barriers to drug delivery. Nature biotechnology. 2015;33(9):941-51.

25. Rodriguez Amado JR, Prada AL, Duarte JL, Keita H, da Silva HR, Ferreira AM, et al. Development, stability and in vitro delivery profile of new loratadine-loaded nanoparticles. Saudi Pharmaceutical Journal. 2017;25(8):1158-68.

26. Feracci H, Gutierrez BS, Hempel W, Gil IS. Organic Nanoparticles. In: de la Fuente JM, Grazu V, editors. Frontiers of Nanoscience. 4: Elsevier; 2012. p. 197-230.

27. Md S, Mustafa G, Baboota S, Ali J. Nanoneurotherapeutics approach intended for direct nose to brain delivery. Drug Development and Industrial Pharmacy. 2015;41(12):1922-34.

28. Sekerdag E, Lüle S, Bozdağ Pehlivan S, Öztürk N, Kara A, Kaffashi A, et al. A potential non-invasive glioblastoma treatment: Nose-to-brain delivery of farnesylthiosalicylic acid incorporated hybrid nanoparticles. Journal of Controlled Release. 2017;261:187-98.

29. El-Zaafarany GM, Soliman ME, Mansour S, Awad GAS. Identifying lipidic emulsomes for improved oxcarbazepine brain targeting: In vitro and rat in vivo studies. International journal of pharmaceutics. 2016;503(1):127-40.

30. Sharma A, Madhunapantula SV, Robertson GP. Toxicological considerations when creating nanoparticle based drugs and drug delivery systems? Expert opinion on drug metabolism & toxicology. 2012;8(1):47-69.

31. Bulbake U, Doppalapudi S, Kommineni N, Khan W. Liposomal Formulations in Clinical Use: An Updated Review. Pharmaceutics. 2017;9(2):1-33.

32. Allen TM, Cullis PR. Liposomal drug delivery systems: From concept to clinical applications. Advanced Drug Delivery Reviews. 2013;65(1):36-48.

33. Immordino ML, Dosio F, Cattel L. Stealth liposomes: review of the basic science, rationale, and clinical applications, existing and potential. International Journal of Nanomedicine. 2006;1(3):297-315.

34. Szebeni J, Bedőcs P, Rozsnyay Z, Weiszhár Z, Urbanics R, Rosivall L, et al. Liposome-induced complement activation and related cardiopulmonary distress in pigs: factors promoting reactogenicity of Doxil and AmBisome. Nanomedicine: Nanotechnology, Biology and Medicine. 2012;8(2):176-84.

35. Huynh NT, Passirani C, Saulnier P, Benoit JP. Lipid nanocapsules: a new platform for nanomedicine. International journal of pharmaceutics. 2009;379(2):201-9.

36. Heurtault B, Saulnier P, Pech B, Benoit JP, Proust JE. Interfacial stability of lipid nanocapsules. Colloids and Surfaces B: Biointerfaces. 2003;30(3):225-35.

37. Heurtault B, Saulnier P, Pech B, Proust JE, Benoit JP. A novel phase inversion-based process for the preparation of lipid nanocarriers. Pharmaceutical Research. 2002;19(6):875-80.

38. Heurtault B, Saulnier P, Pech B, Venier-Julienne MC, Proust JE, Phan-Tan-Luu R, et al. The influence of lipid nanocapsule composition on their size distribution. European journal of pharmaceutical sciences : official journal of the European Federation for Pharmaceutical Sciences. 2003;18(1):55-61.

39. Vonarbourg A, Passirani C, Saulnier P, Simard P, Leroux JC, Benoit JP. Evaluation of pegylated lipid nanocapsules versus complement system activation and macrophage uptake. Journal of Biomedical Materials Research Part A. 2006;78A(3):620-8.

40. Vonarbourg A, Passirani C, Saulnier P, Benoit JP. Parameters influencing the stealthiness of colloidal drug delivery systems. Biomaterials. 2006;27(24):4356-73.

41. Vonarbourg A, Saulnier P, Passirani C, Benoit JP. Electrokinetic properties of noncharged lipid nanocapsules: influence of the dipolar distribution at the interface. Electrophoresis. 2005;26(11):2066-75.

42. Le Roux G, Moche H, Nieto A, Benoit JP, Nesslany F, Lagarce F. Cytotoxicity and genotoxicity of lipid nanocapsules. Toxicology in Vitro. 2017;41:189-99.

43. Maupas C, Moulari B, Béduneau A, Lamprecht A, Pellequer Y. Surfactant dependent toxicity of lipid nanocapsules in HaCaT cells. International journal of pharmaceutics. 2011;411(1):136-41.

44. Kumari A, Yadav SK, Yadav SC. Biodegradable polymeric nanoparticles based drug delivery systems. Colloids and Surfaces B: Biointerfaces. 2010;75(1):1-18.

45. Makadia HK, Siegel SJ. Poly Lactic-co-Glycolic Acid (PLGA) as Biodegradable Controlled Drug Delivery Carrier. Polymers. 2011;3(3):1377-97.

46. Wu XS, Wang N. Synthesis, characterization, biodegradation, and drug delivery application of biodegradable lactic/glycolic acid polymers. Part II: Biodegradation. Journal of Biomaterials Science, Polymer Edition. 2001;12(1):21-34.

47. Govender T, Stolnik S, Garnett MC, Illum L, Davis SS. PLGA nanoparticles prepared by nanoprecipitation: drug loading and release studies of a water soluble drug. Journal of Controlled Release. 1999;57:171-85.

48. Xu P, Gullotti E, Tong L, Highley CB, Errabelli DR, Hasan T, et al. Intracellular drug delivery by poly(lactic-co-glycolic acid) nanoparticles, revisited. Molecular pharmaceutics. 2009;6(1):190-201.

49. Jain D, Athawale R, Bajaj A, Shrikhande S, Goel PN, Gude RP. Studies on stabilization mechanism and stealth effect of poloxamer 188 onto PLGA nanoparticles. Colloids and Surfaces B: Biointerfaces. 2013;109:59-67.

50. Li J-T, Caldwell KD, Rapoport N. Surface Properties of Pluronic-Coated Polymeric Colloids. Langmuir. 1994;10(12):4475-82.

51. Redhead HM, Davis SS, Illum L. Drug delivery in poly(lactide-co-glycolide) nanoparticles surface modified with poloxamer 407 and poloxamine 908: in vitro characterisation and in vivo evaluation. Journal of Controlled Release. 2001;70(3):353-63.

52. Wang Y, Jiang S, Wang H, Bie H. A mucoadhesive, thermoreversible in situ nasal gel of geniposide for neurodegenerative diseases. PloS one. 2017;12(12):1-17.

53. Kozlov MY, Melik-Nubarov NS, Batrakova EV, Kabanov AV. Relationship between Pluronic Block Copolymer Structure, Critical Micellization Concentration and Partitioning Coefficients of Low Molecular Mass Solutes. Macromolecules. 2000;33(9):3305-13.

54. Bhatia S. Nanoparticles Types, Classification, Characterization, Fabrication Methods and Drug Delivery Applications. In: Bhatia S, editor. Natural Polymer Drug Delivery Systems: Nanoparticles, Plants, and Algae. Cham: Springer International Publishing; 2016. p. 33-93.

55. Wong IY, Bhatia SN, Toner M. Nanotechnology: emerging tools for biology and medicine. Genes & development. 2013;27(22):2397-408.

56. Andar AU, Hood RR, Vreeland WN, DeVoe DL, Swaan PW. Microfluidic Preparation of Liposomes to Determine Particle Size Influence on Cellular Uptake Mechanisms. Pharmaceutical Research. 2014;31(2):401-13.

57. Zhang S, Li J, Lykotrafitis G, Bao G, Suresh S. Size-Dependent Endocytosis of Nanoparticles. Advanced materials 2009;21:419-24.

58. Kim TH, Kim M, Park HS, Shin US, Gong MS, Kim HW. Size-dependent cellular toxicity of silver nanoparticles. Journal of biomedical materials research Part A. 2012;100(4):1033-43.

59. Pan Y, Neuss S, Leifert A, Fischler M, Wen F, Simon U, et al. Size-dependent cytotoxicity of gold nanoparticles. Small. 2007;3(11):1941-9.

60. Rothen-Rutishauser B, Mühlfeld C, Blank F, Musso C, Gehr P. Translocation of particles and inflammatory responses after exposure to fine particles and nanoparticles in an epithelial airway model. Particle and Fibre Toxicology. 2007;4(1):9.

61. Walkey CD, Olsen JB, Guo H, Emili A, Chan WCW. Nanoparticle Size and Surface Chemistry Determine Serum Protein Adsorption and Macrophage Uptake. Journal of the American Chemical Society. 2012;134(4):2139-47.

62. Hoo CM, Starostin N, West P, Mecartney ML. A comparison of atomic force microscopy (AFM) and dynamic light scattering (DLS) methods to characterize nanoparticle size distributions. Journal of Nanoparticle Research. 2008;10(S1):89-96.

63. Bootz A, Vogel V, Schubert D, Kreuter J. Comparison of scanning electron microscopy, dynamic light scattering and analytical ultracentrifugation for the sizing of poly(butyl cyanoacrylate) nanoparticles. European Journal of Pharmaceutics and Biopharmaceutics. 2004;57(2):369-75.

64. Xu R. Progress in nanoparticles characterization: Sizing and zeta potential measurement. Particuology. 2008;6(2):112-5.

65. He C, Hu Y, Yin L, Tang C, Yin C. Effects of particle size and surface charge on cellular uptake and biodistribution of polymeric nanoparticles. Biomaterials. 2010;31(13):3657-66.

66. Musumeci T, Pellitteri R, Spatuzza M, Puglisi G. Nose-to-brain delivery: evaluation of polymeric nanoparticles on olfactory ensheathing cells uptake. Journal of Pharmaceutical Sciences. 2014;103(2):628-35.

67. Jones MC, Jones SA, Riffo-Vasquez Y, Spina D, Hoffman E, Morgan A, et al. Quantitative assessment of nanoparticle surface hydrophobicity and its influence on pulmonary biocompatibility. Journal of Controlled Release. 2014;183:94-104.

68. Xiao Y, Wiesner MR. Characterization of surface hydrophobicity of engineered nanoparticles. Journal of Hazardous Materials. 2012;215-216:146-51.

69. Gessner A, Waicz R, Lieske A, Paulke BR, Mäder K, Müller RH. Nanoparticles with decreasing surface hydrophobicities: influence on plasma protein adsorption. International journal of pharmaceutics. 2000;196(2):245-9.

70. Saptarshi SR, Duschl A, Lopata AL. Interaction of nanoparticles with proteins: relation to bio-reactivity of the nanoparticle. Journal of Nanobiotechnology. 2013;11:26-.

71. Ljungh A, Wadstrom T. Salt aggregation test for measuring cell surface hydrophobicity of urinary Escherichia coli. European journal of clinical microbiology. 1982;1(6):388-93.

72. Santander-Ortega MJ, Jódar-Reyes AB, Csaba N, Bastos-González D, Ortega-Vinuesa JL. Colloidal stability of Pluronic F68-coated PLGA nanoparticles: A variety of stabilisation mechanisms. Journal of Colloid and Interface Science. 2006;302(2):522-9.

73. Nag A, Mitra G, Ghosh PC. A colorimetric assay for estimation of polyethylene glycol and polyethylene glycolated protein using ammonium ferrothiocyanate. Analytical biochemistry. 1996;237(2):224-31.

74. Salatin S, Maleki Dizaj S, Yari Khosroushahi A. Effect of the surface modification, size, and shape on cellular uptake of nanoparticles. Cell biology international. 2015;39(8):881-90.

75. Skandrani N, Barras A, Legrand D, Gharbi T, Boulahdour H, Boukherroub R. Lipid nanocapsules functionalized with polyethyleneimine for plasmid DNA and drug co-delivery and cell imaging. Nanoscale. 2014;6(13):7379-90.

76. Dulieu C, Bazile D. Influence of Lipid Nanocapsules Composition on Their Aptness to Freeze-Drying. Pharmaceutical Research. 2005;22(2):285-92.

77. Sempf K, Arrey T, Gelperina S, Schorge T, Meyer B, Karas M, et al. Adsorption of plasma proteins on uncoated PLGA nanoparticles. European Journal of Pharmaceutics and Biopharmaceutics. 2013;85(1):53-60.

78. Moghimi SM, Hunter AC. Poloxamers and poloxamines in nanoparticle engineering and experimental medicine. Trends in Biotechnology. 2000;18(10):412-20.

79. Stolnik S, Garnett MC, Davies MC, Illum L, Bousta M, Vert M, et al. The colloidal properties of surfactant-free biodegradable nanospheres from poly(β-malic acid-co-benzyl malate)s and poly(lactic acid-co-glycolide). Colloids and Surfaces A: Physicochemical and Engineering Aspects. 1995;97(3):235-45.

80. Gentile P, Chiono V, Carmagnola I, Hatton PV. An Overview of Poly(lactic-co-glycolic) Acid (PLGA)-Based Biomaterials for Bone Tissue Engineering. International Journal of Molecular Sciences. 2014;15(3):3640-59.

81. Dong WY, Körber M, López Esguerra V, Bodmeier R. Stability of poly(d,l-lactide-co-glycolide) and leuprolide acetate in in-situ forming drug delivery systems. Journal of Controlled Release. 2006;115(2):158-67.

82. Fonseca C, Simões S, Gaspar R. Paclitaxel-loaded PLGA nanoparticles: preparation, physicochemical characterization and in vitro anti-tumoral activity. Journal of Controlled Release. 2002;83(2):273-86.

83. Oliveira CL, Veiga F, Varela C, Roleira F, Tavares E, Silveira I, et al. Characterization of polymeric nanoparticles for intravenous delivery: Focus on stability. Colloids and Surfaces B: Biointerfaces. 2017;150:326-33.

84. Santander-Ortega MJ, Csaba N, Alonso MJ, Ortega-Vinuesa JL, Bastos-González D. Stability and physicochemical characteristics of PLGA, PLGA:poloxamer and

PLGA:poloxamine blend nanoparticles: A comparative study. Colloids and Surfaces A: Physicochemical and Engineering Aspects. 2007;296(1):132-40.

85. Lu H, Li J, Li M, Gong T, Zhang Z. Systemic delivery of alpha-asarone with Kolliphor HS 15 improves its safety and therapeutic effect on asthma. Drug Delivery. 2015;22(3):266-75.

86. Tirosh O, Barenholz Y, Katzhendler J, Priev A. Hydration of polyethylene glycol-grafted liposomes. Biophysical Journal. 1998;74(3):1371-9.

87. Sadeghi R, Jahani F. Salting-In and Salting-Out of Water-Soluble Polymers in Aqueous Salt Solutions. The Journal of Physical Chemistry B. 2012;116(17):5234-41.

88. Zhang M, Yang B, Liu W, Li S. Influence of hydroxypropyl methylcellulose, methylcellulose, gelatin, poloxamer 407 and poloxamer 188 on the formation and stability of soybean oil-in-water emulsions. Asian Journal of Pharmaceutical Sciences. 2017;12(6):521-31.

89. Gao H. Progress and perspectives on targeting nanoparticles for brain drug delivery. Acta Pharmaceutica Sinica B. 2016;6(4):268-86.

90. Kovalevich J, Langford D. Considerations for the use of SH-SY5Y neuroblastoma cells in neurobiology. Methods in molecular biology (Clifton, NJ). 2013;1078:9-21.

91. Bi C, Wang A, Chu Y, Liu S, Mu H, Liu W, et al. Intranasal delivery of rotigotine to the brain with lactoferrin-modified PEG-PLGA nanoparticles for Parkinson's disease treatment. International Journal of Nanomedicine. 2016;11:6547-59.

92. Ternchoocheep K, Surangkul D, Ysothonsreekul S. The recovery and protective effects of asiatic acid on differentiated human neuroblastoma SH-SY5Y cells cytotoxic-induced by cholesterol. Asian Pacific Journal of Tropical Biomedicine. 2017;7(5):416-20.

93. Yang Y, Yu Y, Wang J, Li Y, Li Y, Wei J, et al. Silica nanoparticles induced intrinsic apoptosis in neuroblastoma SH-SY5Y cells via CytC/Apaf-1 pathway. Environmental Toxicology and Pharmacology. 2017;52:161-9.

94. Owens DE, Peppas NA. Opsonization, biodistribution, and pharmacokinetics of polymeric nanoparticles. International journal of pharmaceutics. 2006;307(1):93-102.

95. Fotakis G, Timbrell JA. In vitro cytotoxicity assays: Comparison of LDH, neutral red, MTT and protein assay in hepatoma cell lines following exposure to cadmium chloride. Toxicology Letters. 2006;160(2):171-7.

96. Stoddart MJ. Cell viability assays: introduction. Methods in molecular biology 2011;740:1-6.

97. Zhang S, Gao H, Bao G. Physical Principles of Nanoparticle Cellular Endocytosis. ACS nano. 2015;9(9):8655-71.

98. Sánchez-Moreno P, Boulaiz H, Ortega-Vinuesa JL, Peula-García JM, Aránega A. Novel Drug Delivery System Based on Docetaxel-Loaded Nanocapsules as a Therapeutic Strategy Against Breast Cancer Cells. International Journal of Molecular Sciences. 2012;13(4):4906-19.

99. Claudia M, Kristin Ö, Jennifer O, Eva R, Eleonore F. Comparison of fluorescence-based methods to determine nanoparticle uptake by phagocytes and non-phagocytic cells in vitro. Toxicology. 2017;378:25-36.

100. Ibuki Y, Toyooka T. Nanoparticle Uptake Measured by Flow Cytometry. In: Reineke J, editor. Nanotoxicity: Methods and Protocols. Totowa, NJ: Humana Press; 2012. p. 157-66.

101. Wesen E, Jeffries GDM, Matson Dzebo M, Esbjorner EKA-Ohoo. Endocytic uptake of monomeric amyloid-beta peptides is clathrin- and dynamin-independent and results in selective accumulation of Abeta(1-42) compared to Abeta(1-40). Scientific Report. 2017;7(2021):1-14.

102. Gu J, Chi M, Sun X, Wang G, Li M, Liu L, et al. Propofol-Induced Protection of SH-SY5Y Cells against Hydrogen Peroxide Is Associated with the HO-1 via the ERK Pathway. International Journal of Medical Sciences. 2013;10(5):599-606.

103. Heinz H, Pramanik C, Heinz O, Ding Y, Mishra RK, Marchon D, et al. Nanoparticle decoration with surfactants: Molecular interactions, assembly, and applications. Surface Science Reports. 2017;72(1):1-58.

104. Chieng YY, Chen SB. Interaction and Complexation of Phospholipid Vesicles and Triblock Copolymers. The Journal of Physical Chemistry B. 2009;113(45):14934-42.

105. Wu G, Lee KYC. Interaction of Poloxamers with Liposomes: An Isothermal Titration Calorimetry Study. The Journal of Physical Chemistry B. 2009;113(47):15522-31.

106. Greenebaum B, Blossfield K, Hannig J, Carrillo CS, Beckett MA, Weichselbaum RR, et al. Poloxamer 188 prevents acute necrosis of adult skeletal muscle cells following high-dose irradiation. Burns. 2004;30(6):539-47.

107. Houang EM, Haman KJ, Filareto A, Perlingeiro RC, Bates FS, Lowe DA, et al. Membrane-stabilizing copolymers confer marked protection to dystrophic skeletal muscle in vivo. Molecular Therapy - Methods & Clinical Development. 2015;2:15042.

108. Salama HA, Mahmoud AA, Kamel AO, Abdel Hady M, Awad GAS. Phospholipid based colloidal poloxamer–nanocubic vesicles for brain targeting via the nasal route. Colloids and Surfaces B: Biointerfaces. 2012;100:146-54.

109. Frey SL, Zhang D, Carignano MA, Szleifer I, Lee KYC. Effects of block copolymer's architecture on its association with lipid membranes: Experiments and simulations. The Journal of Chemical Physics. 2007;127(11):114904.

110. Staiger K, Staiger H, Weigert C, Haas C, Haring HU, Kellerer M. Saturated, but not unsaturated, fatty acids induce apoptosis of human coronary artery endothelial cells via nuclear factor-kappaB activation. Diabetes. 2006;55(11):3121-6.

111. Lacoeuille F, Garcion E, Benoit JP, Lamprecht A. Lipid nanocapsules for intracellular drug delivery of anticancer drugs. Journal of Nanoscience and Nanotechnology. 2007;7:1-6.

112. Passerini N, Craig DQM. An investigation into the effects of residual water on the glass transition temperature of polylactide microspheres using modulated temperature DSC. Journal of Controlled Release. 2001;73(1):111-5.

113. Paillard A, Hindré F, Vignes-Colombeix C, Benoit J-P, Garcion E. The importance of endo-lysosomal escape with lipid nanocapsules for drug subcellular bioavailability. Biomaterials. 2010;31(29):7542-54.

114. Drasler B, Vanhecke D, Rodriguez-Lorenzo L, Petri-Fink A, Rothen-Rutishauser B. Quantifying nanoparticle cellular uptake: which method is best? Nanomedicine. 2017;12(10):1095-9.

115. Simonsson C, Bastiat G, Pitorre M, Klymchenko AS, Bejaud J, Mely Y, et al. Inter-nanocarrier and nanocarrier-to-cell transfer assays demonstrate the risk of an immediate unloading of dye from labeled lipid nanocapsules. European Journal of Pharmaceutics and Biopharmaceutics. 2016;98:47-56.

116. Bastiat G, Pritz CO, Roider C, Fouchet F, Lignières E, Jesacher A, et al. A new tool to ensure the fluorescent dye labeling stability of nanocarriers: A real challenge for fluorescence imaging. Journal of Controlled Release. 2013;170(3):334-42.

117. Klymchenko AS, Roger E, Anton N, Anton H, Shulov I, Vermot J, et al. Highly lipophilic fluorescent dyes in nano-emulsions: towards bright non-leaking nano-droplets. RSC advances. 2012;2(31):11876-86.

118. Petters C, Dringen R. Accumulation of iron oxide nanoparticles by cultured primary neurons. Neurochemistry International. 2015;81:1-9.

119. Vilella A, Tosi G, Grabrucker AM, Ruozi B, Belletti D, Vandelli MA, et al. Insight on the fate of CNS-targeted nanoparticles. Part I: Rab5-dependent cell-specific uptake and distribution. Journal of Controlled Release. 2014;174:195-201.

120. Rejman J, Oberle V, S. ZI, Hoekstra D. Size-dependent internalization of particles via the pathways of clathrin- and caveolae-mediated endocytosis. Biochemical Journal. 2004;377:159-69.

121. Amin FU, Shah SA, Badshah H, Khan M, Kim MO. Anthocyanins encapsulated by PLGA@PEG nanoparticles potentially improved its free radical scavenging capabilities via p38/JNK pathway against Aβ1–42-induced oxidative stress. Journal of Nanobiotechnology. 2017;15(1):12.

122. Umerska A, Matougui N, Groo A-C, Saulnier P. Understanding the adsorption of salmon calcitonin, antimicrobial peptide AP114 and polymyxin B onto lipid nanocapsules. International journal of pharmaceutics. 2016;506(1):191-200.

# 6. Supplementary information

## 6.1 Calibration curve for excess surfactant assay

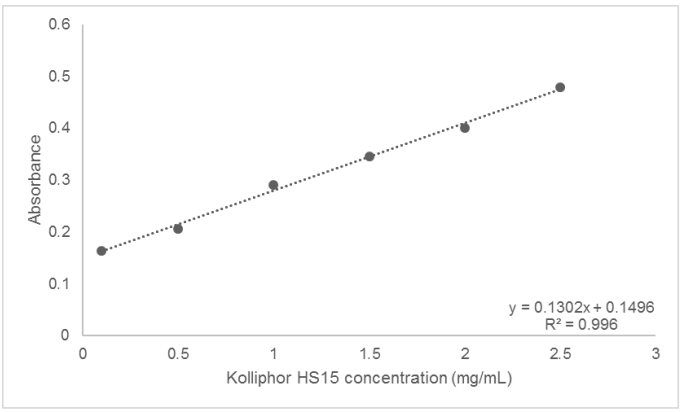


(a)

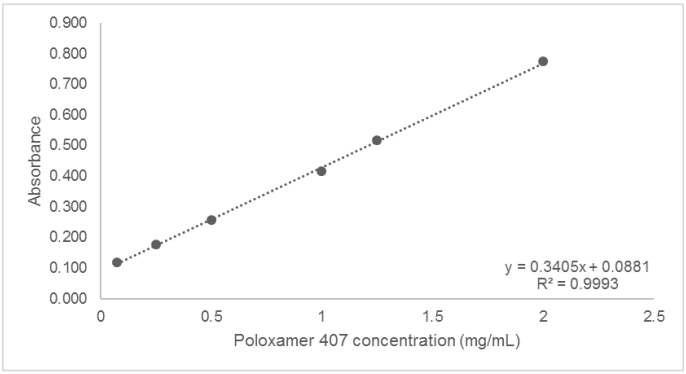


(b)

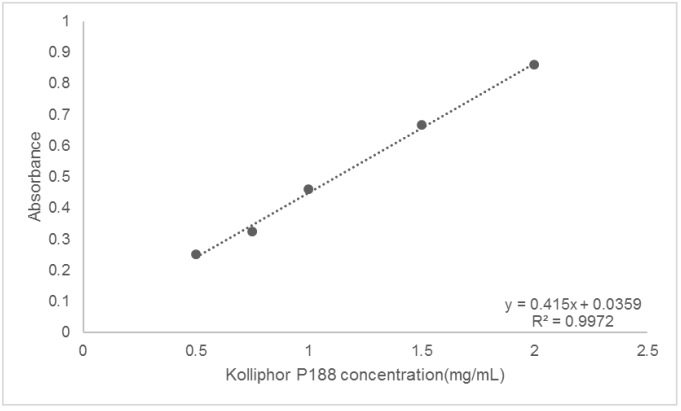


(c)

**Figure S1.** Calibration curve for quantification of excess surfactants: (a) Kolliphor® HS15, (b) Poloxamer 407, and (c) Kolliphor® P188

Example of the calculation to obtain LOD and LOQ values based on ICH guidelines:

Kolliphor® HS15

| Conc (mg/mL) | Response 1 | Response 2 | Response 3 | Average response (Y) | True response (Yi) | Y-Yi | $(Y-Yi)^2$ |
|---|---|---|---|---|---|---|---|
| 0.1 | 0.17 | 0.164 | 0.159 | 0.164333333 | 0.16262 | 0.001713 | 2.93551E-06 |
| 0.5 | 0.191 | 0.219 | 0.21 | 0.206666667 | 0.2147 | -0.00803 | 6.45344E-05 |
| 1 | 0.285 | 0.291 | 0.294 | 0.29 | 0.2798 | 0.0102 | 0.00010404 |
| 1.5 | 0.336 | 0.348 | 0.355 | 0.346333333 | 0.3449 | 0.001433 | 2.05444E-06 |
| 2 | 0.398 | 0.396 | 0.408 | 0.400666667 | 0.41 | -0.00933 | 8.71111E-05 |
| 2.5 | 0.461 | 0.466 | 0.511 | 0.479333333 | 0.4751 | 0.004233 | 1.79211E-05 |
| | | | | | | Σ | 0.000278597 |
| | | | | | | Σ/(n-2) | 6.96492E-05 |
| | | | | | | σ | 0.008345607 |

where
Σ = sums of $(Y-Yi)^2$
n = number of samples
σ = standard deviation of responses (square root of (Σ/(n-2))

$$\text{Limit of detection (LoD)} = \frac{3.3 \text{ x } \sigma}{\text{slope of the calibration curve}} = \frac{3.3 \text{ x } 0.008345607}{0.1302} = \mathbf{0.211\ mg/mL}$$

$$\text{Limit of quantification (LoQ)} = \frac{10 \text{ x } \sigma}{\text{slope of the calibration curve}} = \frac{10 \text{ x } 0.008345607}{0.1302} = \mathbf{0.641\ mg/mL}$$

## 6.2 Cytotoxicity of Kolliphor® HS15 following 1-hour exposure

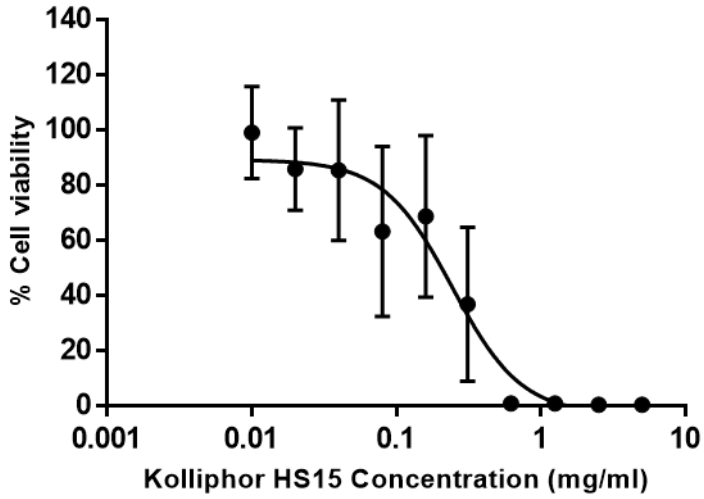


**Figure S2.** Cell viability of SH-SY5Y cells following 1-hour exposure of Kolliphor® HS15

**Table S1.** IC50 of Kolliphor® HS15 towards SH-SY5Y cells following 1-hour exposure

| Exposure time (h) | IC50 |
|---|---|
| 1 | 0.225 ± 0.11 |

Data presented as mean ± SD from at least three independent experiments